Title
Geometric current response in Chern systems and topological delocalization in Floquet class AIII systems

Author
Brown, Albert

Publication Date
2019

Peer reviewed|Thesis/dissertation

UNIVERSITY OF CALIFORNIA
Los Angeles

Geometric current response in Chern systems and topological delocalization in Floquet class AIII systems

A dissertation submitted in partial satisfaction
of the requirements for the degree
Doctor of Philosophy in Physics

by

Albert Nikola Brown

2019

ABSTRACT OF THE DISSERTATION

Geometric current response in Chern systems
and topological delocalization in Floquet class AIII systems

by

Albert Nikola Brown
Doctor of Philosophy in Physics
University of California, Los Angeles, 2019
Professor Rahul Roy, Chair

Topological phases are phases of matter that are characterized by discrete quantities known as topological invariants. This thesis explores two such phases, the static Chern insulator phase (symmetry class A) in two dimensions and the dynamical Floquet chiral phase (symmetry class AIII) in one dimension.

A Chern insulator is a gapped single particle system on a lattice with a non-zero first Chern number for some of its energy-momentum bands. We consider subjecting a Chern insulator to a non-uniform external electric field. The response is band geometric which means it is robust to deformations of the energy bands which do not cause band touchings. We find a connection between this response and previous work on band geometric quantities.

A Floquet insulator is a unitary time evolved system defined by a time periodic Hamiltonian. We first describe an existing model of a 1D chain with 2D onsite Hilbert space and chiral symmetry. Then we introduce a disordered model of the system and look at how its topological properties are robust to the disorder. We find a power law scaling of $\nu = 2$ for the localization-delocalization transition of the eigenstates of the unitary operator as the drive evolves towards the midway point of its evolution.

The dissertation of Albert Nikola Brown is approved.

Sudip Chakravarty

Hong-Wen Jiang

Eric D'Hoker

Rahul Roy, Committee Chair

University of California, Los Angeles

2019

"We do what we can because we must."

TABLE OF CONTENTS

LIST OF FIGURES

LIST OF TABLES

ACKNOWLEDGMENTS

I would like to thank everyone who helped me get to where I am. Graduate school is an equal parts frustrating and exciting endeavor, and I'm glad for everyone that followed me on this journey.

My advisor, Rahul Roy, for leading our group's vision. Fenner Harper, our post-doc, as a collaborator, a mentor, and a friend. The rest of our graduate research group for being a team and a community: Dominic, Xu, Pratik, as well as David of Roy group emeritus. My friends, Alex and Hunter, as well, for keeping these years fun and graciously losing to me at board games (and maybe winning a few) as well as the many other friends in the department who created the supportive work environment we have.

Finally, but most importantly, I wouldn't be where I am without my partner in crime for life, Melody, and all the ways she has brightened my life.

VITA

2013	B.S. Physics, Carnegie Mellon University
2014	M.S. Physics, UCLA

PUBLICATIONS AND PRESENTATIONS

A. Brown, F. Harper, and R.Roy. *Critical exponent of delocalization transition in topological chiral 1D Floquet chains*, in preparation

A. Brown*, "Band geometry and Chern insulator inhomogeneous electric response"
APS March Meeting, Los Angeles Convention Center
March 08, 2018

A. Brown*, "Band geometry and electrical response of Chern insulators."
APS March Meeting, New Orleans E. N. Morial Convention Center
March 14, 2017

CHAPTER 1

Introduction and Overview

The concept of topological properties in condensed matter physics has redefined how we consider the classification of phases of matter. Instead of being characterized by the spontaneous breaking of a symmetry, a topological phases are characterized by discrete quantities known as topological invariants. Topological phases have applications to a significant amount of condensed matter physics. The main application is insulator physics which we will discuss in this paper, but they can also exist in superconductors [QZ11, LW16], semimetals [AMV18], cold atoms [CDS19], optics [OPA19], and others, some still to be discovered. Even though a number of these topics started as purely theoretical models, all I mentioned have seen a matching field of experimental research and realization.

One large advantage that has continued to motivate and advance this field of research is the implications of the discrete nature of the invariant. As there is no halfway for a topological phase, one can make very strong statements about a phase's robustness to disorder [HK10], universality [Kit09], or stability [Kit03]. This makes it a powerful tool in studying condensed matter systems.

In my research I have considered both static and dynamical properties of single particle (non-interacting) Chern Insulators and Floquet Topological Insulators. Chern insulators started as a set of toy model systems to understand the quantum Hall effect without external magnetic field, but grew to be its own field of study. Floquet physics is the time dependent extension of static topological insulating systems and realizes physics unique to its dynamics.

The thesis as follows will be organized as so. Chapter 2 will give a pedagogical and historical background on quantum Hall and the development of the field of topological phases.

Chapter 3 will study band geometrical properties and present my research on non-uniform Chern insulator current response. Chapter 4 introduces Floquet topological phases and talks about their properties and classification. Chapter 5 gives my research on disordered Floquet evolutions and the localization properties of their eigenstates.

CHAPTER 2

Topological Phases

2.1 Classical Hall

We start by considering the movement of an electron in a uniform magnetic field, $\vec{B}$ which can be said, without loss of generality, to point in the $\hat{z}$ direction, $\vec{B} = B\hat{z}$. The Lorentz force from the field acts perpendicular to the motion of the electron,

$$\vec{F}_\ell = e\vec{v} \times \vec{B} = \vec{F}_c = \frac{mv^2}{r}$$

This perpendicular force acts as a centripetal force that moves the electron in a circular orbit normal to the direction of the magnetic field. The resulting angular frequency of the motion, known as the cyclotron frequency, is independent of the velocity of the particle,

$$r = \frac{mv}{eB} \Rightarrow \omega_c = \frac{v}{r} = \frac{eB}{m}$$

This frequency will be the B-dependent constant that sets the energy scale of our problem.

Writing down the Lagrangian,

$$\mathcal{L} = \frac{m\dot{r}^2}{2} + e\vec{A} \cdot \dot{\vec{r}}$$

we can find the form of the canonical momentum,

$$\vec{p} = \frac{\partial \mathcal{L}}{\partial \dot{\vec{r}}} = m\dot{\vec{r}} + e\vec{A}$$

where we see that $\vec{A}$, the vector potential, enters. Using this form, we can write down the Hamiltonian for the system

$$H = \frac{1}{2m_e}(\vec{p} - e\vec{A})^2$$

From here we can approach the quantum problem.

2.2 Landau Levels

Given the canonical commutation relations, we can see that the kinetic momentum, $\vec{\Pi}$, do not commute with each other,

$$[\Pi_x, \Pi_y] = [p_x - eA_x, p_y - eA_y] = ie\hbar(\nabla_x A_y - \nabla_y A_x) = ie\hbar B_z$$

Given this, we can form creation and annihilation operators,

$$a = (2e\hbar B)^{-\frac{1}{2}}(\Pi_x + i\Pi_y)$$

$$a^\dagger = (2e\hbar B)^{-\frac{1}{2}}(\Pi_x - i\Pi_y)$$

where the normalization is the inverse of what was found above to ensure that $[a, a^\dagger] = 1$. Inverting these equations, we get,

$$\Pi_x = \sqrt{\frac{e\hbar B}{2}}(a + a^\dagger)$$

$$\Pi_y = -i\sqrt{\frac{e\hbar B}{2}}(a - a^\dagger)$$

and plugging this into our Hamiltonian, we see that we are left with a quantum harmonic oscillator with frequency ω_c,

$$H = \hbar\omega_c(a^\dagger a + \frac{1}{2})$$

These equispaced energy levels are known as Landau levels. Unlike a harmonic oscillator, however, we have a two dimensional system, and therefore another set of operators, as well as the gauge freedom inherent to the vector potential to consider before we can write down the wavefunctions.

2.3 Choice of Gauge

Because of the gauge freedom in the vector potential,

$$\vec{A}(\vec{r}) \to \vec{A}(\vec{r}) + \vec{\nabla}\phi(\vec{r})$$

there are many equivalent ways to write our kinetic momentum operators. There are two common choices given a constant B field, the Landau gauge and the rotationally symmetric gauge.

2.3.1 Landau Gauge

Choosing $A = (0, Bx)$ is a simple choice to give a constant out of plane magnetic field. With this choice, a significant simplification of the Hamiltonian occurs.

$$H = \frac{p_x^2}{2m} + \frac{1}{2m}(p_y - eBx)^2$$

We see here that p_y commutes with the Hamiltonian, so the two operators are mutually diagonalizable and we can substitute the operator with its eigenvalue, k_y.

$$H = \frac{p_x^2}{2m} + \frac{1}{2m}(\hbar k_y - eBx)^2 = \frac{p_x^2}{2m} + \frac{1}{2}m\omega_c^2(x - \frac{\hbar k_y}{m\omega_c})^2$$

We see that we have the harmonic oscillator Hamiltonian just as when we used ladder operators. We also notice translational symmetry along the y direction. The Landau gauge

is therefore sometimes referred to as the translationally invariant gauge. Our eigenstates can be simply written down as a combination of solutions to the harmonic oscillator and translationally invariant plane waves,

$$\Psi_{n,k_y}(\vec{r}) = e^{ik_y y}\psi_n(x - \frac{\hbar k_y}{m\omega_c})$$

where the ψ_n is the nth harmonic oscillator wave function. This form is exponentially localized along the x-direction and completely delocalized along the y-direction as will be relevant in later discussion.

Additionally, we see that the position of the harmonic oscillator is offset by a momentum dependent factor. Returning to the statement of the Hamiltonian, we can think of writing it in terms of the center of the harmonic oscillator.

$$H = \frac{\vec{\Pi}^2}{2m_e} = \frac{1}{2}m\omega_c^2(x - X)^2 + \frac{1}{2}m\omega_c^2(y - Y)^2$$

where the new cyclotron center operators are,

$$X = x + \frac{\Pi_y}{m\omega_c} \quad \text{and} \quad Y = y - \frac{\Pi_x}{m\omega_c}$$

These center of position operators also do not commute with each other. Additionally, both of them commute with Π_x and Π_y,

$$[\Pi_x, X] = [\Pi_x, x] + \frac{1}{m\omega_c}[\Pi_x, \Pi_y] = -i\hbar + \frac{1}{m\omega_c}i\hbar eB = 0$$
$$[\Pi_y, Y] = [\Pi_y, y] + \frac{1}{m\omega_c}[\Pi_y, \Pi_x] = -i\hbar - \frac{1}{m\omega_c}(-i\hbar eB) = 0$$

where the $[\Pi_y, X]$ and $[\Pi_x, Y]$ commutators are trivially zero. This means we can create a distinct set of creation and annihilation operators for X, Y.

$$b = \sqrt{\frac{eB}{2\hbar}}(X - iY)$$

$$b^\dagger = \sqrt{\frac{eB}{2\hbar}}(X + iY)$$

so we can specify eigenstates of the Hamiltonian as harmonic oscillator states in two indices. The b index, however, doesn't contribute any energy, so there is a massive degeneracy to our system. To see the structure of the degenerate subspace, we consider the rotationally symmetric gauge.

2.3.2 Rotationally Symmetric Gauge

If we chose a symmetric vector potential, $A = (-By/2, Bx/2)$, then our eigenstates are rotationally symmetric. First consider the form of the creation and annihilation operators,

$$\begin{aligned} a &= (2e\hbar B)^{-\frac{1}{2}}(\Pi_x + i\Pi_y) = (2e\hbar B)^{-\frac{1}{2}}[-i\hbar(\nabla_x + i\nabla_y) - \frac{ieB}{2}(x + iy)] \\ &= -i\sqrt{\frac{\hbar}{2eB}}(2\frac{\partial}{\partial \bar{z}} + \frac{eB}{2\hbar}z) \end{aligned}$$

where we have used the substitution of the complex variable $z = x + iy$. A factor of two is required so that the derivative $\frac{\partial}{\partial z}z = 1$ and vice versa. We then have our two independent variables be z and $\bar{z}$, as can be seen by taking the partial derivative,

$$\frac{\partial}{\partial \bar{z}}z = \frac{1}{2}(\nabla_x + i\nabla_y)(x + iy) = 0$$

and again, similarly vice versa. Also we can find $a^\dagger$ just by complex conjugation,

$$a^\dagger = -i\sqrt{\frac{\hbar}{2eB}}(2\frac{\partial}{\partial z} - \frac{eB}{2\hbar}\bar{z})$$

Now, finding the ground state is as simple as looking for solutions to the equation,

$$a|\Psi\rangle = 0 = -i\sqrt{\frac{\hbar}{2eB}}(2\frac{\partial}{\partial \bar{z}} + \frac{eB}{2\hbar}z)\Psi(z, \bar{z})$$

for which there are an entire family of solutions,

$$\Psi(z,\bar{z}) = p(z)e^{-eB\bar{z}z/4\hbar}$$

The function $p(z)$ can be any analytic complex function, we choose a basis of polynomials, $\{z^m\}$ to represent them. The normalization of these functions is then related to m

$$N_m = \frac{1}{\sqrt{m!\pi}}\left(\frac{eB}{2\hbar}\right)^{\frac{m+1}{2}}$$

To make sense of the index m within the scope of the problem, we calculate the action of the b or $b^\dagger$ operators on a wavefunction of this form. In terms of the new variables, our operators are

$$b = \sqrt{\frac{eB}{2\hbar}}(X - iY) = \sqrt{\frac{\hbar}{2eB}}(2\frac{\partial}{\partial z} + \frac{eB}{2\hbar}\bar{z})$$

$$b^\dagger = \sqrt{\frac{\hbar}{2eB}}(-2\frac{\partial}{\partial \bar{z}} + \frac{eB}{2\hbar}z)$$

so if we take

$$\begin{aligned} b\Psi_{0,m}(z,\bar{z}) &= \sqrt{\frac{\hbar}{2eB}}(2\frac{\partial}{\partial z} + \frac{eB}{2\hbar}\bar{z})N_m z^m e^{-eB\bar{z}z/4\hbar} \\ &= m\sqrt{\frac{\hbar}{2eB}}N_m z^{m-1}e^{-eB\bar{z}z/4\hbar} = \sqrt{m}\Psi_{0,m-1}(z,\bar{z}) \end{aligned}$$

we see that the power of m is just the index of the ladder state for the $b, b^\dagger$ operators. The 0 index here is just denoting that we are using the function for the lowest energy state, also referred to as the Lowest Landau Level or LLL. Now that we have solved for the eigenstates, we can refer to them compactly using a ket of their a and b ladder operator eigenvalues, $|n,m\rangle$.

To understand the massive degeneracy in each Landau level, consider the action of the angular momentum operator on $\Psi_{0,m}$. The angular momentum operator L_z can be written in complex variables as

$$
\begin{aligned}
L_z &= xp_y - yp_x = -i\hbar(x\nabla_y - y\nabla_x) = \\
&= \frac{z+\bar{z}}{2} i(\frac{\partial}{\partial z} - \frac{\partial}{\partial \bar{z}}) - \frac{z-\bar{z}}{2i}(\frac{\partial}{\partial z} + \frac{\partial}{\partial \bar{z}}) \\
&= \hbar(z\frac{\partial}{\partial z} - \bar{z}\frac{\partial}{\partial \bar{z}})
\end{aligned}
$$

We can then translate our complex variables into creation and annihilation operators,

$$z = \sqrt{\frac{2\hbar}{eB}}(b^\dagger + ia)$$

$$\frac{\partial}{\partial z} = \sqrt{\frac{eB}{8\hbar}}(b + ia^\dagger)$$

$$\bar{z} = \sqrt{\frac{2\hbar}{eB}}(b - ia^\dagger)$$

$$\frac{\partial}{\partial \bar{z}} = -\sqrt{\frac{eB}{8\hbar}}(b^\dagger - ia)$$

so that we can write L_z as

$$
\begin{aligned}
L_z &= \frac{1}{2}\hbar\Big[(b^\dagger + ia)(b + ia^\dagger) + (b - ia^\dagger)(b^\dagger - ia)\Big] \\
&= \frac{1}{2}\hbar\Big[b^\dagger b - aa^\dagger + bb^\dagger - a^\dagger a\Big] \\
&= \hbar(b^\dagger b - a^\dagger a)
\end{aligned}
$$

so state $\Psi_{n,m}$ will have angular momentum $\hbar(m-n)$. However, this is not a physical quantity, the "higher" degenerate states within a Landau level are not actually spinning faster. This is because the form of the angular momentum was written in terms of canonical momentum and not the kinetic momentum. Therefore this number is dependent on the fact that we chose the rotationally symmetric gauge.

If we calculate kinetic angular momentum instead, we see each state only has $-(2n+1)\hbar$ of angular momentum,

$$\begin{aligned} x\Pi_y - y\Pi_x &= x(p_y - \frac{eB}{2}x) - y(p_x + \frac{eB}{2}y) = L_z - \frac{eB}{2}\bar{z}z \\ &= \hbar(b^\dagger b - a^\dagger a) - \hbar(b^\dagger + ia)(b - ia^\dagger) \\ &= -\hbar(2a^\dagger a + 1) + i\hbar(b^\dagger a^\dagger - ab) \end{aligned}$$

with the second set of terms not giving a contribution to the expectation value on any eigenstate. This is consistent with the state having only rotational kinetic energy given by $\frac{1}{2}\omega L$.

From here, we can make an approximate statement about the degeneracy of these Landau levels. For the kinetic angular momentum, we calculated the term $\bar{z}z = r^2$. As we are dealing with a very large number of states, we can think of looking at the largest value of m such that it's peak distance, $\langle r^2 \rangle$, is contained within some finite system size radius R. Given this, we find that

$$r^2_{max} \approx \langle \bar{z}z \rangle = \frac{2\hbar}{eB}\langle (b^\dagger + ia)(b - ia^\dagger) \rangle = \frac{2\hbar}{eB}(m_{max} + n + 1)$$

We can safely drop the $n + 1$ from the expression as they will both be of order 1 in any applicable case, as we care to study low energy systems. Given this, we can then compare to our system size and see that

$$m_{max} \approx \frac{eBR^2}{2\hbar} = \frac{e\Phi}{h}$$

where Φ is the total magnetic flux piercing the system. Due to the presence of h, this will be an enormous number for a system in a macroscopic magnetic field.

Despite starting with relatively simple assumptions, Landau levels have shown to be a rich quantum system. In the next section we will see its applications as a model for the Integer Quantum Hall Effect.

2.4 Integer Quantum Hall Effect (IQHE)

The Integer Quantum Hall Effect (henceforth IQHE) was first seen by Wakabayashi and Kawji in 1978.[WK78] They looked at MOSFET transistors under high magnetic fields and saw small plateaus of the transverse Voltage while, at the same time, the longitudinal Voltage through the device went to zero. Shortly after in 1980, von Klitzing, with samples prepared by Dorda and Pepper, saw plateaux in the transverse Voltage at exactly quantized values[KDP80]. One can talk about the transverse or Hall conductivity $\sigma_{xy} = \frac{J}{V_H}$, computed from the experimental voltage and induced current. From there we can define a Hall resistivity ρ_{xy} as well as a longitudinal resistivity ρ_{xx}, data for which can be seen in figure 2.1.

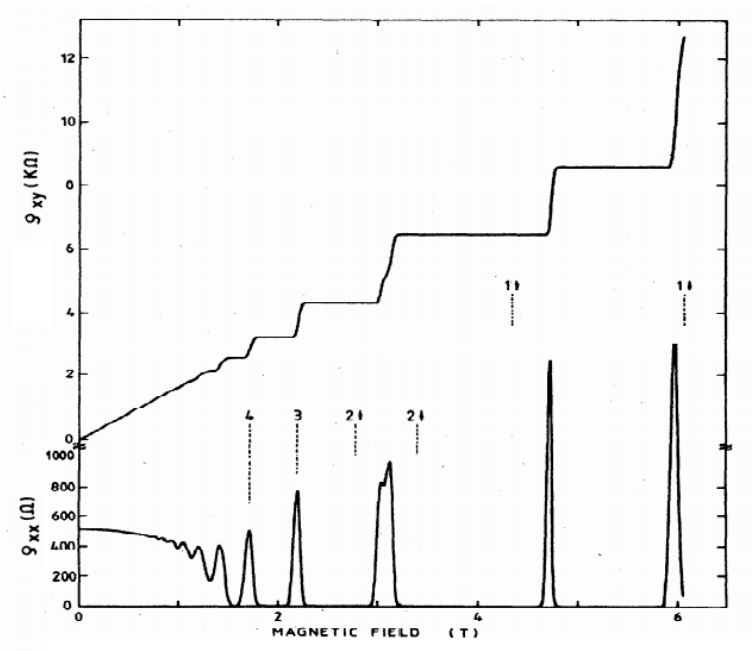

Figure 2.1: Here is data by von Klitzing on an Aluminum doped Gallium Arsenide heterostructure at fixed carrier density, presented for his Nobel Prize acceptance in 1985[Kli86]. The plateaux are incredibly flat and corresponded exactly with the current response of an integer number of filled Landau levels.

The plateaux of transverse (or Hall) conductivity occur at integer multiples of a quantity

similar to the one we found at the end of the previous section

$$\sigma_H = \sigma_{xy} = \frac{e^2\nu}{h}$$

where ν is the plateau index. Also called the filling fraction, ν corresponds to the number of filled Landau levels in a model of our system. Like our statement of the Landau level degeneracy, the result depends on the constant $\frac{e}{h} = \phi_o$ which is referred to as the flux quantum.

The flatness and broadness of the plateaux can be understood by acknowledging the presence of disorder. As shown by Aoki and Ando[AA81], disorder broadens the Landau level bands, but also localizing all states except those close to the central Landau level energy. The effect of this is that shifting the relative placement of the Fermi energy to the conducting states when you are in a plateau by changing the magnetic field only causes population of localized states. When the Fermi level passes through the extended, Landau level-like portion of the density of states, there is a quick increase up to the next plateau. A cartoon picture of this process can be seen in figure 2.2.

To understand the exact quantization of the plateau conductance, Laughlin explains that the current can only exist in integer increments of the flux quantum[Lau81]. The argument, later refined by Halperin[Hal82], considers bending a finite two dimensional Landau level system into a loop, for example by adding periodic boundary conditions in one of our spatial directions. The current due to a potential drop V across the non periodic direction of our system can be seen as the change in the system energy as a function of adiabatic insertion of magnetic flux through the loop.

$$I \propto \frac{\partial E}{\partial \Phi} = \frac{1}{L}\frac{\partial E}{\partial A}$$

and due to the simplicity of the Landau level problem, we can consider a uniform vector potential A_x in the direction of the loop and write the derivative in terms of ∂A. However the effect of a change ΔA_x caused by the insertion of flux is to shift the phase of the wavefunction in a spatially dependent way.

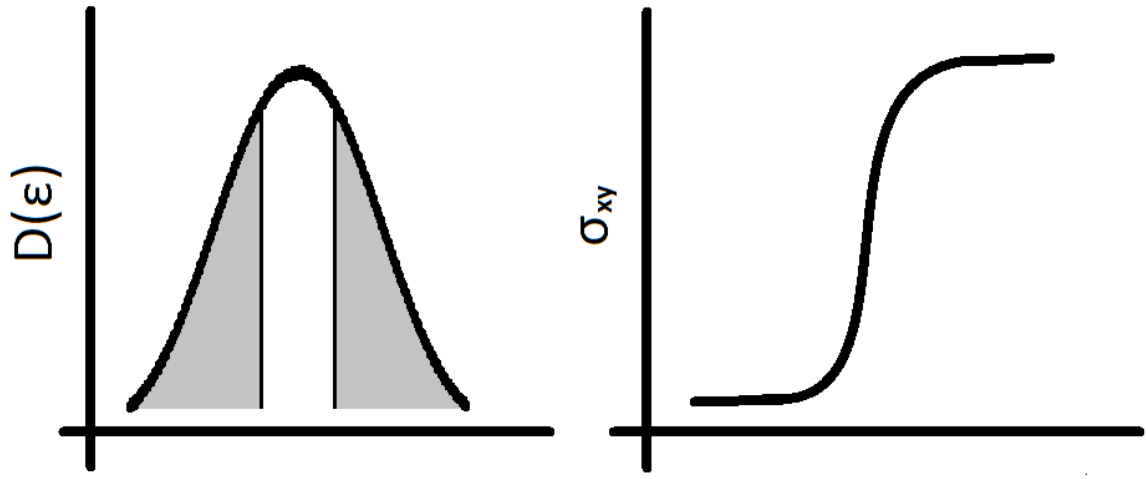

Figure 2.2: This shows a cartoon picture of the effect of disorder on a Landau level. The top picture shows the density of states after disorder breaks the degeneracy and localizes states in the shaded region. The right picture shows the effect of this on a linear response calculation of the conductivity which becomes the transition from one plateau to the next.

$$\Psi \to e^{iex\Delta A_x/\hbar}\Psi$$

For localized disordered states, this poses no issue, but for the extended Landau level states that are required for conduction, the change must be by an amount

$$\Delta A = n\frac{h}{eL}$$

so that the wavefunction phase is correct at the periodic boundary.

A transformation by this amount is a gauge invariance of the system and the current then has to come from the motion of n electrons from one edge to the other, which is a current of

$$I = \frac{neV}{L\Delta A} = \frac{ne^2V}{h}$$

which gives the conductance seen in the experiment. It should be noted that these arguments break down in the presence of interactions which become important when the conducting

bands are not fully filled. This spawned its own Nobel prize winning field of the fractional quantum Hall effect which is beyond the scope of this thesis[TSG82, STG99].

2.5 Chern Insulators

The next major step in understanding the integer quantization came by Thouless, Kohmoto, Nightingale, and den Nijs in 1982[TKN82]. Starting from the Kubo formula linear response as used by Aoki and others[AA81, Pra81, Tho81], they showed a proof for the quantization in linear response. The Kubo formula is a general statement of conductivity given by the linear response of an applied external electric field.

$$\sigma_H \propto \sum_{\substack{E_\alpha \leq E_f \\ E_f < E_\beta}} \frac{\langle \frac{\partial H}{\partial k_1} \rangle_{\alpha\beta} \langle \frac{\partial H}{\partial k_2} \rangle_{\beta\alpha} - \langle \frac{\partial H}{\partial k_2} \rangle_{\alpha\beta} \langle \frac{\partial H}{\partial k_1} \rangle_{\beta\alpha}}{(E_\alpha - E_\beta)^2}$$

The sum is taken over energy states by separating states below the Fermi energy (E_α) and states above it (E_β). The braket notation denotes the matrix element of the operator between energy eigenstates $|\alpha\rangle$ and $|\beta\rangle$. Due to how Landau levels function in the presence of disorder, we expect the Fermi level to be in a mobility gap of disordered states between conducting Landau levels, so α here will be Landau level states from filled bands and β will be higher energy unfilled states. The different crystal momentum, k_1 and k_2, merely refer to two different basis vector directions in our 2D system, making no additional assumptions to the structure of our Hamiltonian or any underlying lattice.

We have assumed some form of translational invariance (discrete or continuous), so we can write the states as Bloch states

$$\Psi_k(\vec{r}) = e^{-i\vec{k}\cdot\vec{r}} u_k(\vec{r})$$

We can also write the derivatives of the Hamiltonian as velocity operators and those as commutators of the position operators and the Hamiltonian.

$$\frac{\partial H}{\partial k_1} \propto v_1 \propto [r_1, H]$$

Plugging this in, we can act the Hamiltonian in the commutator on our states and cancel the energy denominator. We are left with an expectation of position operators

$$\sigma_H \propto \sum_{E_\alpha \leq E_f < E_\beta} \Big(\langle \alpha | r_1 | \beta \rangle \langle \beta | r_2 | \alpha \rangle - \langle \alpha | r_2 | \beta \rangle \langle \beta | r_1 | \alpha \rangle \Big)$$

Since we have eliminated the energy denominator, we can look at the sum and see that if we included states such that $\beta = \alpha$, that part of the sum would be zero as there would be a corresponding right term to cancel each left term. Therefore we can add in those states to the sum and take out the sum over β as a complete set of states. If we write the states in terms of our Bloch wave functions, the position operators are equivalent to k derivatives of the periodic part.

$$\sigma_H \propto \frac{1}{2\pi} \sum \int d^2k \int d^2r \Big(\frac{\partial u^*}{\partial k_1} \frac{\partial u}{\partial k_2} - \frac{\partial u^*}{\partial k_2} \frac{\partial u}{\partial k_1} \Big)$$

where the sum is now just over independent filled bands and the integrals come from writing the wavefunctions in Bloch form. Using Stokes theorem, we can write this expression as a loop integral around the edge of the Brillouin zone.

$$\sigma_H \propto \frac{1}{4\pi} \sum \oint dk_j \int d^2r \Big(u^* \frac{\partial u}{\partial k_j} - \frac{\partial u^*}{\partial k_j} u \Big)$$

As the wavefunction is analytic, this is equivalent to the winding number of the phase around the Brillouin zone. Therefore the conductivity must be quantized. However, an important part here is the minimal amount of assumptions about our system that were required. The analytic machinery at the end of this derivation is completely independent of the IQHE. The only serious assumption we made was one of independent non-overlapping bands as well as the initial one neglecting interactions.

In the next few years, Berry [Ber84] and Simon [Sim83] codify and update the mathematics of Chern [Che46] to give language to this geometric property of a system, geometric meaning computable from only the wavefunctions and their derivatives. The principle building block is the Berry connection of the periodic part of a wavefunction $u_n(k)$ over momentum

$$\vec{A}_n(\vec{k}) = i \langle u_n(\vec{k}) | \vec{\nabla}_k | u_n(\vec{k}) \rangle$$

This is a vector potential and therefore gauge dependent on the choice of phase of the wavefunction. However, if we look at the path integral of this quantity along a curve $\mathcal{C}(t)$, the integral, known as the Berry phase, is gauge independent if the path forms a loop

$$\gamma_n = i \int_{\mathcal{C}(t_i)}^{\mathcal{C}(t_f)} dt \langle u_n(\vec{k}) | \vec{\nabla}_k | u_n(\vec{k}) \rangle$$

$$|u_n(\vec{k})\rangle \to e^{i\theta(\vec{k})} |u_n(\vec{k})\rangle$$

$$\gamma_n(t) \to \gamma_n(t) + \theta(t) - \theta(t_i)$$

so over a loop, $\theta(t_f)$ and $\theta(t_i)$ will always cancel as they are the same point.

Additionally, we can define the Berry curvature

$$-i\mathcal{F}_n(\vec{k}) = \vec{\nabla}_k \times A_n(\vec{k}) = \left\langle \frac{\partial u_n(\vec{k})}{\partial k_x} \middle| \frac{\partial u_n(\vec{k})}{\partial k_y} \right\rangle - \left\langle \frac{\partial u_n(\vec{k})}{\partial k_y} \middle| \frac{\partial u_n(\vec{k})}{\partial k_x} \right\rangle$$

which is the integrand of above when performing a Stokes theorem transformation. Note that this is working backwards along the same formula considered by TKNN. However, this curvature form not only gives us the same Kubo formula, but also an equivalent statement of the first Chern number of our space of wavefunctions

$$\iint_{\text{B.Z.}} d^2\vec{k} \;\; \mathcal{F}_n(\vec{k}) = 2\pi i C_n$$

This quantity is a quantized topological invariant which means that deformations of the wavefunctions will not change it so long as they do not destroy the assumptions of isolated (non-crossing) energy bands and periodicity. Shortly after the publication of this description Kohmoto translated the results for the IQHE into the Chern formalism [Koh85]. The Chern number of each Landau level is shown to be one.

A comprehensive example of a Chern band model was explored by Haldane [Hal88] who adapted a model described by Semenoff [Sem84] and showed an example of a model that has non-zero Chern number without the presence of an external magnetic field. The model is one evocative of graphene and describes a single particle tight binding model on a hexagonal lattice denoted by $\vec{R}$. The unit cell on a hexagonal lattice contains two sites, here labeled

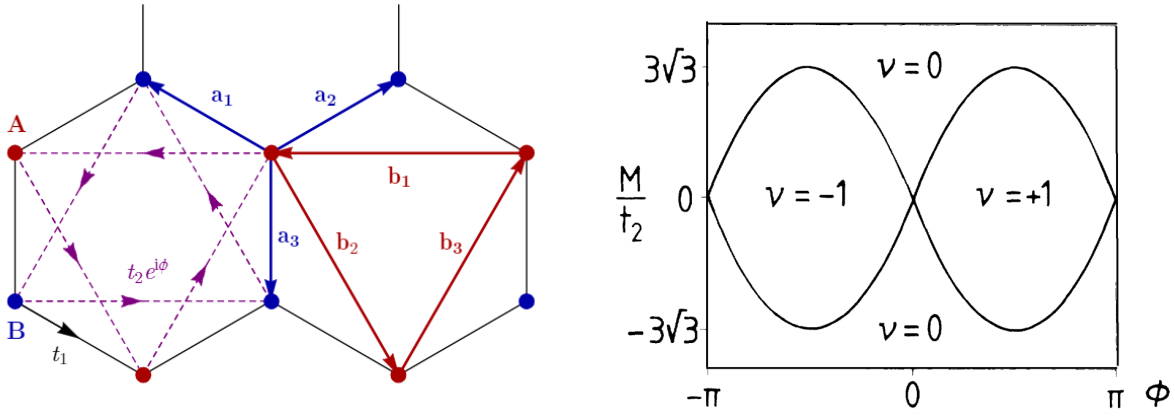

(a) (b)

Figure 2.3: A visualization of the Haldane model. Fig 2.3a shows the hoppings and the lattice vectors including the winding direction of the phase. Fig 2.3b shows the phase diagram where the ratio $\frac{M}{t_2}$ assumes $t_1 = 1$. The indices ν correspond to the Chern number of the bottom band in that phase [Hal88].

A and B with respective creation and annihilation operators $c_A(\vec{r})$ and $c_B(\vec{r})$ respectively, acting at a site $\vec{r}$. The Hamiltonian is as follows

$$\begin{aligned} H = &\sum_{\vec{r}\in\vec{R}}\sum_i t_1\left[c_B^\dagger(\vec{r}+\vec{a_i})c_A(\vec{r}) + c_A^\dagger(\vec{r}+\vec{a_i})c_B(\vec{r})\right] \\ &+ \sum_j t_2\left[e^{\pm i\phi}c_A^\dagger(\vec{r}\pm\vec{b_j})c_A(\vec{r}) + e^{\mp i\phi}c_B^\dagger(\vec{r}\pm\vec{b_j})c_B(\vec{r})\right] \\ &+ M\left[c_A^\dagger(\vec{r})c_A(\vec{r}) - c_B^\dagger(\vec{r})c_B(\vec{r})\right] \end{aligned}$$

where the $\{a_i\}$ and $\{b_j\}$ are the NN and NNN lattice vectors respectively for the specified lattice site and t_1 and t_2 are their hopping strengths. The idea behind the model is if we assume that even without a magnetic field the underlying structure of the lattice can cause fluctuations around zero in the magnetic flux even though the net flux through a cell remains zero. NN hoppings traverse a hexagonal loop, enclosing net zero flux, but the NNN hops cut through only part of the cell pick up the phase $\pm\phi$ depending on the direction of the winding. This phase factor breaks time reversal invariance. Finally, the term M is a splitting between the sites within a unit cell.

The solution of this Hamiltonian is a gapped two band spectrum for all but a specific dividing curve in parameter space. If the Fermi level is put in the gap, we can calculate σ_{xy} and find the phase diagram in figure 2.3. Not only is there a quantized conductance as in the IQHE without needing an external magnetic field, but by adjusting the parameters of the phase and the relative strengths of the splitting and NNN hopping, we see that the transport physics is unchanged despite having different wave function solutions except for the exact points where the two bands touch. This Chern Insulator (CI) shows that the key aspects of the IQHE that were necessary for quantized conductance was a gapped multi-band model (so as to be able to use the Berry phase formalism) with time reversal invariance breaking. Haldane referred to this effect as a parity anomaly (after the effect in 2+1 D electromagnetism [NN81]) and it is also known as the anomalous quantum Hall effect.

The Chern number we see in the Haldane model is of the bottom filled band. In each phase, the top band has an opposite Chern number. Generally, the Chern numbers of a system are such that a fully occupied system has Chern number zero. The IQHE appears a notable exception with each Landau level contributing a Chern number of 1, though it has an infinite number of energy bands in the model as it stands, so occupying every band is impossible. In fact, partially filling a Landau level and turning on perturbations or interactions split band into subbands who still have a net Chern number 1 [TKN82, Str82]. This does not accurately model experimental findings for the fractional quantum Hall effect[TSG82, STG99] a fundamentally different description is needed. For this reason, we will not consider the interactions between particles. Instead we consider the classification of Chern insulators within the broader category of topological phases protected by symmetry.

2.6 Classification of Topological Phases

2.6.1 Other Topological Insulators

While you cannot talk about topological phases in terms of the traditional language of spontaneous symmetry breaking phase transitions, symmetry is still important in understanding

the universality of topological phases. A topological phase is defined by an integer valued order parameter called a topological invariant, named so because its integer nature means it cannot change through continuous deformations of the band structure. Instead, it (and therefore the phase of the system) can only change by the discrete event of the touching of energy bands. The calculation of a Chern number is zero if the bands can be mapped into each other by some symmetry (described in detail below) as the Chern numbers must cancel. However the topological invariant need not always be a Chern number of the band.

A good example is topological insulators (TIs) which are similar to Chern insulators in that they have conducting edge modes except they do not break time reversal symmetry. Proposed by Kane and Mele[KM05a], they first considered graphene as it had spin orbit coupling that was predicted to be necessary in initial investigations of the subject[SCN04] so that spin and current could be related in a way to maintain time reversal symmetry. In their explanation of the theory, Kane and Mele define an invariant in terms of the Pfaffian of matrix elements of the time reversal operator[KM05b]. This effect was seen shortly afterward in HgTe quantum wells[KWB07, RBB09]. The invariant was later expressed in a constructive manner based on the projector onto the filled band[Roy09]. Because of time reversal invariance, this projector could be split into two projectors that are mapped onto each other by time reversal symmetry

$$P(\vec{k}) = P_1(\vec{k}) + P_2(\vec{k})$$

$$P_1(\vec{k}) = \Theta P_2(-\vec{k})\Theta^{-1}$$

where Θ is the time reversal operator. While the choice of P_1 and P_2 were not unique, the Chern number of each modulo 2 was a topological invariant equivalent to the one defined by Kane and Mele and was not dependent on the way P_1 and P_2 were chosen. This is notably different than Chern insulators as there was only two possible values for the topological invariant while Chern bands could have any integer Chern number.

This band projector approach was then expanded to time reversal invariant 3D systems [Roy10, FKM07] to define 3D topological insulators. The Dirac cones describing conducting

modes in these systems have spin-momentum locking to preserve time reversal invariance. Unlike Chern insulators that hadn't seen a non-trivial example in 3D systems, TIs seemed present in 2D and 3D. Additionally, there was the difference in available topological indices. Therefore there seemed a relation between available symmetries and available topological phases that required further explanation.

2.6.2 The Periodic Table

We have looked at the band structure of every Hamiltonian to calculate topological invariants. Therefore we are interested in global symmetries that map the band structure onto itself. This means that we have 3 main symmetries to consider: time reversal (Θ), particle/hole or parity (P), and chiral symmetry (C). Up to a unitary rotation, these can be expressed as

$$\Theta H(\vec{k})\Theta^{-1} = H^*(-\vec{k})$$
$$PH(\vec{k})P^{-1} = -H^*(-\vec{k})$$
$$CH(\vec{k})C^{-1} = -H(\vec{k})$$

Both P and Θ have a freedom of sign in the square of the operator, giving each two possible forms. Space group symmetries are not considered here, but classification of topological phases based on the crystal symmetries as well as band symmetries has been a recent field of the study of topological crystalline insulators[AF15, CTS16].

Given these symmetries, we can define equivalency classes of Hamiltonians based on what combinations of these symmetries they posses. The three symmetries are not completely independent, however

$$PTH(\vec{k})T^{-1}P^{-1} = PH^*(-\vec{k})P^{-1} = -H(\vec{k}) = CH(\vec{k})C^{-1}$$

so any system with two symmetries will have the third, resulting in 10 total classes. These are labeled by letter Altland-Zirnbauer classes which correspond to each combination of these symmetries[AZ97]. By identifying the homotopy groups of the classifying space of the

Clifford algebras corresponding to our 10 symmetry groups, Kitaev classified the possible phases available for each symmetry class in any system dimension [Kit09]. This created a "Periodic Table" for topological phases shown in table 2.1. The group shown for each entry shows the space of indices is either trivial ($\emptyset$), 1 or 0 ($\mathbb{Z}_2$), or any integer ($\mathbb{Z}$). One result is that any Hamiltonian in a topological phase can be continuously deformed to resemble any other one with the same symmetries and dimension. Chern insulator systems correspond to class A while TIs correspond to class AII, finally elucidating their differences.

class	Θ	P	C	d=0	1	2	3	4	5	6	7
A				$\mathbb{Z}$	$\emptyset$	$\mathbb{Z}$	$\emptyset$	$\mathbb{Z}$	$\emptyset$	$\mathbb{Z}$	$\emptyset$
AIII			1	$\emptyset$	$\mathbb{Z}$	$\emptyset$	$\mathbb{Z}$	$\emptyset$	$\mathbb{Z}$	$\emptyset$	$\mathbb{Z}$
AI	+1			$\mathbb{Z}$	$\emptyset$	$\emptyset$	$\emptyset$	$\mathbb{Z}$	$\emptyset$	$\mathbb{Z}_2$	$\mathbb{Z}_2$
BDI	+1	+1	1	$\mathbb{Z}_2$	$\mathbb{Z}$	$\emptyset$	$\emptyset$	$\emptyset$	$\mathbb{Z}$	$\emptyset$	$\mathbb{Z}_2$
D		+1		$\mathbb{Z}_2$	$\mathbb{Z}_2$	$\mathbb{Z}$	$\emptyset$	$\emptyset$	$\emptyset$	$\mathbb{Z}$	$\emptyset$
DIII	-1	+1	1	$\emptyset$	$\mathbb{Z}_2$	$\mathbb{Z}_2$	$\mathbb{Z}$	$\emptyset$	$\emptyset$	$\emptyset$	$\mathbb{Z}$
AII	-1			$\mathbb{Z}$	$\emptyset$	$\mathbb{Z}_2$	$\mathbb{Z}_2$	$\mathbb{Z}$	$\emptyset$	$\emptyset$	$\emptyset$
CII	-1	-1	1	$\emptyset$	$\mathbb{Z}$	$\emptyset$	$\mathbb{Z}_2$	$\mathbb{Z}_2$	$\mathbb{Z}$	$\emptyset$	$\emptyset$
C		-1		$\emptyset$	$\emptyset$	$\mathbb{Z}$	$\emptyset$	$\mathbb{Z}_2$	$\mathbb{Z}_2$	$\mathbb{Z}$	$\emptyset$
CI	+1	-1	1	$\emptyset$	$\emptyset$	$\emptyset$	$\mathbb{Z}$	$\emptyset$	$\mathbb{Z}_2$	$\mathbb{Z}_2$	$\mathbb{Z}$

Table 2.1: The periodic classification of topological phases. Each class has a ± 1 for each present symmetry operator based on the square of the operator. Chiral symmetry cannot square to -1 here. The topological invariants of the phases belong to the representation of the groups for each specific combination of symmetry and dimension. For $d \geq 8$ the pattern repeats as dictated by Bott periodicity[Bot59].

CHAPTER 3

Current Per Wannier Orbital Response

3.1 Context and Overview

3.1.1 Band Geometry

Related to topological quantities is the concept of band geometric quantities. A band geometric quantity is a function that is defined across the Brillouin zone and depends only on the form of the momentum space wave functions. This means it does not depend on the energy of the wave function, and is only made up of expectations of k-space derivatives. One may notice that this definition applies to the Berry curvature and connection, but not the Chern number, making geometric quantities a superset to topological quantities.

An important application of geometric quantities is in projected density operators. The properties of these operators for the lowest Landau level Hamiltonian were studied and used by Girvin, MacDonald, and Platzman who defined them in terms of a commutator algebra (the GMP algebra) [GMP86]

$$[\bar{\rho}_{\gamma,\vec{q}_1}, \bar{\rho}_{\gamma,\vec{q}_2}] = 2i \exp\Big(\frac{\vec{q}_1 \cdot \vec{q}_2 \ell^2}{2}\Big) \sin\Big(\frac{\hat{z} \cdot (\vec{q}_1 \times \vec{q}_2) l^2}{2}\Big) \bar{\rho}_{\gamma,\vec{q}_1+\vec{q}_2}$$

where $\bar{\rho}_q = \hat{P}_\gamma \rho_q \hat{P}_\gamma$ is the momentum space density operator projected, $\hat{P}$, onto a specific band indexed by γ. The magnetic length ℓ is the length scale of the Landau level, defined by the magnitude of the magnetic field, $\ell^2 = \frac{\hbar}{e|B|}$. They projected fractional quantum Hall states onto the lowest Landau level so as to compute a single mode approximation of the many body gap. However, the algebraic structure they created to relate quantities of this type had further reaching applications.

Roy et. al. [PRS12, Roy14] considered these projected density operators for Chern insulators to see if the same algebra holds in the low energy limit to discuss the low energy physics of fractional Chern insulators. What they found is that, provided the Berry curvature of the system was sufficiently flat to be replaced by its average, $\bar{B}$, the algebra would hold to order q^2 with $\bar{B}$ replacing l_B^2 from the Landau level. To hold to order q^3 and higher, an additional band geometric quantity, the Fubini-Study metric ($g_{\alpha\beta}$) must be flat in the Brillouin zone as well.

$$g_{\alpha\beta} = 1/2\Big(\Big\langle\frac{\partial u_k}{\partial\vec{k}_\alpha}\Big|\frac{\partial u_k}{\partial\vec{k}_\beta}\Big\rangle + \Big\langle\frac{\partial u_k}{\partial\vec{k}_\beta}\Big|\frac{\partial u_k}{\partial\vec{k}_\alpha}\Big\rangle$$
$$- \Big\langle\frac{\partial u_k}{\partial\vec{k}_\alpha}\Big|u_k\Big\rangle\Big\langle u_k\Big|\frac{\partial u_k}{\partial\vec{k}_\beta}\Big\rangle - \Big\langle\frac{\partial u_k}{\partial\vec{k}_\beta}\Big|u_k\Big\rangle\Big\langle u_k\Big|\frac{\partial u_k}{\partial\vec{k}_\alpha}\Big\rangle\Big)$$

The Fubini-Study metric can be seen as a compliment to the Berry curvature as they are the symmetric and anti-symmetric parts (respectively), or alternatively real and imaginary parts of the curvature tensor

$$\mathcal{R}_{\alpha\beta} = \mathrm{Tr}[P_\gamma r_\alpha Q_\gamma r_\beta P_\gamma]$$

where $Q_\gamma = \mathbf{1} - P_\gamma$ and P_γ is the projector on a single band as defined above. Written in the language of projectors, we obtain similarly compact descriptions of $\mathcal{F}$ and g

$$\mathcal{F}_{\alpha,\beta} = \frac{1}{2i}\mathrm{Tr}[P_\gamma r_\alpha Q_\gamma r_\beta P_\gamma - P_\gamma r_\beta Q_\gamma r_\alpha P_\gamma]$$

$$g_{\alpha,\beta} = \frac{1}{2}\mathrm{Tr}[P_\gamma r_\alpha Q_\gamma r_\beta P_\gamma + P_\gamma r_\beta Q_\gamma r_\alpha P_\gamma]$$

In this chapter we will consider the electric response and conductivity of Chern insulators within the language of geometric quantities.

3.1.2 Hall Viscosity

Another place where geometrical effects have been relevant is in the study of semiclassical electron fluids. Avron et. al. described a notion of viscosity for quantum fluids and calculated it for quantum Hall systems [ASZ95]. The antisymmetric component of this viscosity, called the Hall viscosity, describes the effect that an external shearing of the electron motion has on transport in Hall systems. It was shown that the Hall viscosity changed only with

the changing of the Chern number and was therefore topological in nature. However, the magnatude of its contribution to transport is geometric as found by Bradlyn et. al. who derived the effect of the Hall viscosity in linear response [BGR12]. They showed that it contributed to the leading non-zero order term in the expansion of the linear current density response to a general non-uniform electric field.

In a 2013 paper, Biswas derived the same response using a semi-classical method in the lowest Landau level [Bis13]. He expanded the response to a spatially inhomogeneous external potential and noticed that the perturbative current response for any single state in the Landau system is also proportional to the Hall viscosity to first subleading order. This semi-classical approach was mirrored by Roy and Harper to find the same response in a fully quantum way for the lowest Landau level and the Hofstadter model in the limit of small flux [HBJ18]. I extended these techniques in calculating the response of a Chern band.

3.2 Current response per state

The main quantity we adopted from Biswas is the current per state. The current response per state is equivalent to looking at the current contributed by a single particle in a specific momentum state in a specific band. Expanding in first order of perturbation theory, denoted by the superscript (1)

$$\langle \hat{j_y} \rangle_n = \langle \psi_n^{(0)} | e\hat{v}_y | \psi_n^{(1)} \rangle + \langle \psi_n^{(1)} | e\hat{v}_y | \psi_n^{(0)} \rangle$$

$$\langle \hat{j_y} \rangle_n = \langle \psi_n | ei[\hat{y}, \hat{H}] \sum_{m \neq n} |\psi_m\rangle \frac{\langle \psi_m | V(\vec{r}) | \psi_n \rangle}{E_m - E_n} + h.c.$$

$$\langle \hat{j_y} \rangle_n = \langle \psi_n | ei\hat{y} \sum_{m \neq n} |\psi_m\rangle \langle \psi_m | V(\vec{r}) | \psi_n \rangle + h.c.$$

we can write the current per state in terms of the perturbing potential. For now, we have abstracted any momentum band structure away into an index m, n. Now, much like in linear response, we assume that the external field form the potential $V(\vec{r})$ varies periodically but very slowly so that a Taylor expansion in wave number of the potential is a valid perturbation around constant potential. Without loss of generality, we can assume that the potential varies

in the direction perpendicular to which we are calculating current per state. We expand the potential about a point X

$$V(x) = \sum_p V^{(p)}(X)\ (\hat{x} - X)^p$$

and similarly split our current per state into a sum of the contributions from each term in the expansion

$$\langle \hat{j_y} \rangle_n = \sum_p \langle \hat{j_y} \rangle_{p,n} =$$

$$= ie \sum_p V^{(p)}(X) \langle \psi_n | \hat{y} \left(\sum_{m \neq n} |\psi_m\rangle\langle\psi_m| \right) (\hat{x} - X)^p |\psi_n\rangle + h.c.$$

The sum in parentheses acts as a projector onto every state except n so we can replace it with $\mathbf{1} - |\psi_n\rangle\langle\psi_n|$ and simplify using the fact that $[\hat{y}, \hat{x}] = 0$

$$\begin{aligned}
\langle \hat{j_y} \rangle_{p,n} &= ieV^{(p)}(X) \langle \psi_n | \hat{y}(\mathbf{1} - |\psi_n\rangle\langle\psi_n|)(\hat{x} - X)^p - (\hat{x} - X)^p(\mathbf{1} - |\psi_n\rangle\langle\psi_n|)\hat{y}|\psi_n\rangle \\
&= ieV^{(p)}(X) \langle \psi_n | [\hat{y}, (\hat{x} - X)^p] - [P_n \hat{y} P_n, P_n (\hat{x} - X)^p P_n] | \psi_n \rangle \\
&= \langle \psi_n | [P_n (\hat{x} - X)^p P_n, P_n \hat{y} P_n] | \psi_n \rangle
\end{aligned}$$

where P_n is different from our band projector as it projects upon the specific state. Until this point we have assumed locality of the basis of wavefunctions to match the local expansion of the Taylor series. To apply this to Chern insulators, we introduce a convenient choice of basis in the form of hybrid Wannier orbitals.

3.3 Hybrid Wannier orbitals

3.3.1 Definition

Our description of current per state can be applied to any complete set of wave functions on the structure of the bands. However, to obtain a valid approximation to the first few orders of the Taylor series, we need to consider a narrow range of $x - X$. When Biswas applied the expansion of the potential semi-classically, he expanded around the center of the classical cyclotron orbit in the translationally invariant gauge to use their localization

along one spatial direction. To mirror that, we construct a set of localized wave functions. Qi describes a map between the Landau level wave functions and what is referred to as hybrid Wannier states [Qi11]. The name comes from the complete set of localized states, introduced by Wannier, and built from Bloch states in a 1 dimensional system [Wan37]. In contrast, hybrid Wannier states are when the Wannier transformation is performed on 2-D Bloch states, $|\Psi\rangle = e^{-i\vec{k}\cdot\vec{r}}|u\rangle$, across one of the spatial dimension to localize it along one direction

$$|R_x, k_y, \gamma\rangle \equiv \sqrt{N}\int dk_x e^{ik_x R_x}|\Psi_{\vec{k},\gamma}\rangle$$
$$= \sqrt{N}\int dk_x e^{-ik_x(x-R_x)}|u_{\vec{k},\gamma}\rangle$$

where R_x in the 1-D Wannier transformation is the center of localization and N is a normalization coefficient. The choice of the x direction in performing the transformation is chosen to match our choice of coordinates for current response, but the transformation is allowed along any direction. Hybrid Wannier functions have the same periodicity of the Bloch functions in the y direction, but are localized at a single point in the x direction. Instead, they are mapped to each other by discrete lattice translations in the x direction and the set of points $\{R_x\}$ index unit cell translations. When the Chern insulator is already a lattice system, this means the hybrid Wannier orbitals will be arranged identically to a slice of the Bravais lattice along the chosen direction.

It should be noted that the traditional Wannier transformation that exponentially localizes in both x and y directions is impossible for a Chern system[Tho84]. The existence of such a basis means that the projected x and y position operators are each valid quantum numbers of the Wannier basis, a constructed property of maximally local Wannier functions. Furthermore, as they are each Hermitian operators and they both share the wannier function as their eigenfunction, they must commute. However this commutation relation

$$[PxP, PyP]$$

is the Berry curvature and therefore, if the Chern number is non-zero, cannot be zero for the operators to commute.

Finally, for a Chern insulator system the center of localization of the Wannier states depends on k_y.

$$\langle R_x k_y | \hat{x} | R_x k_y \rangle = R_x + \theta(k_y)$$
$$\theta(k_y) = \int_0^{2\pi} dp_x \langle p_x, k_y | \nabla_{p_x} | p_x, k_y \rangle$$

If we consider a unit cell with periodic boundary conditions (i.e. on a torus), for a non-zero Chern number, a full translation in k_y across the Brillouin zone winds a number of times around the torus equal to the Chern number. Therefore, we can combine R_x and k_y to index Wannier orbitals localized at every x position along the system by defining $K_y = k_y + 2\pi R_x$.

3.3.2 Localization and Gauge

A subtlety that was not addressed in the definition of the Wannier transform was that it does not preserve the invariance of the Bloch functions under a $\vec{k}$ dependent phase change. This means the set of Wannier states are not unique and instead depends on a gauge choice in the Bloch functions. Each choice of phase for the Bloch wave functions changes the extent to which the Wannier orbitals are localized. To see this, consider the spread of a Wannier orbital, as defined by Marzari and Vanderbilt [MV97]

$$\Omega \equiv \sum_\gamma [\langle r^2 \rangle_\gamma - \langle \vec{r} \rangle_\gamma^2]$$

Where γ as well as m and n are band indices. We can separate it into a gauge invariant part

$$\Omega_I = \sum_\gamma [\langle r^2 \rangle_\gamma - \sum_{R_x, m} |\langle R_x m | \vec{r} | 0n \rangle|^2]$$

And a gauge dependent one

$$\tilde{\Omega} = \sum_{R_x, m \neq 0n} |\langle R_x m | \vec{r} | 0n \rangle|^2$$

In momentum space, the expectation value can be written as

$$\langle R_x m | \vec{r} | 0n \rangle = i\sqrt{N} \int d\vec{k} e^{ik_x R_x} \langle u_{\vec{k}n} | \vec{\nabla}_k | u_{\vec{k}n} \rangle$$

where it is apparent how an arbitrary k-dependent phase factor would add additional terms. The gauge dependent term is obviously positive definite, so a with a gauge choice that

eliminates it, the Wannier orbitals would be maximally localized. As Vanderbilt et. al. showed, this choice is equivalent to choosing each $|Rn\rangle$ to be an eigenfunction of the projected position operator, $P\hat{x}P|Rn\rangle = R|Rn\rangle$. This eliminates the term as Wannier functions at different R are orthogonal. Other than the superficial degrees of freedom of ordering, choice of origin for R_x, and overall phase, the maximally localized Wannier orbitals are unique.

The gauge independence of Ω_I may not be obvious, but when we rearrange the term slightly

$$\begin{aligned}\Omega_I &= \sum_\gamma \langle \hat{r} \cdot \Big(I - \sum_{R_x m} |R_x m\rangle\langle R_x m| \Big) \cdot \hat{r} \rangle_\gamma \\ &= \sum_\gamma \sum_a \langle P_\gamma \hat{r}_a Q_\gamma \hat{r}_a P_\gamma \rangle\end{aligned}$$

it can be written as a trace of band projectors which are themselves manifestly gauge invariant. One may also note that this term is proportional to the trace of the quantum metric.

3.4 Current per hybrid Wannier orbital

We can now look at calculating current per hybrid Wannier orbital by expanding the potential around the center of the chosen orbital. Because the state is exponentially localized to that position, the Taylor series becomes a valid approximation even to low orders. Without loss of generality, we can choose the point we expand $V(x)$ around to be the center of the 0^{th} unit cell of our Wannier states. We can then write the response to an order p of the expansion in V in terms of the Bloch states under the integral of the Wannier transform as so

$$\begin{aligned}\langle \hat{j_y} \rangle^{(p)} = \frac{eV^{(p)}(R_x)}{i^p} \int dk_x \langle u_k | \frac{\partial}{\partial \vec{k}_y} \Big(|u_k\rangle\langle u_k| \frac{\partial^p}{\partial \vec{k}_x^p} |u_k\rangle \Big) \\ - \langle u_k | \frac{\partial^p}{\partial \vec{k}_x^p} \Big(|u_k\rangle\langle u_k| \frac{\partial}{\partial \vec{k}_y} |u_k\rangle \Big) \\ \equiv \frac{eV^{(p)}(R_x)}{i^p} \int dk_x \mathcal{J}_y^p\end{aligned}$$

The details of this calculation are shown in the appendix 3.A. The band geometric quantity $\mathcal{J}_y^p$ is connected to the greater structure of the GMP algebra. We can see this by separating

its gauge dependent and gauge invariant parts. To construct a similar gauge independent term, we consider the projector trace

$$Tr[\Big[Px^mP, PyP\Big]] \equiv \mathbb{J}_y^m$$

This term is manifestly gauge independent as the only information about the state is in terms of a projector, where any gauge transform will cancel. Writing our integrand expressions $\mathcal{J}_y^p$ expanded at each order in p (calculated in appendix 3.B.3) in terms of $\mathbb{J}_y^m$ we find a general expression

$$\mathcal{J}_y^1 = \mathbb{J}_y^1 = B$$

$$\mathcal{J}_y^2 = \mathbb{J}_y^2 - 2\Big\langle \frac{\partial u}{\partial k_x}\Big| u\Big\rangle \mathcal{J}_y^1 = \mathbb{J}_y^2 + 2A_x\mathbb{J}_y^1$$

$$\mathcal{J}_y^3 = \mathbb{J}_y^3 - 3\Big\langle \frac{\partial u}{\partial k_x}\Big| u\Big\rangle \mathcal{J}_y^2 - 3\Big\langle \frac{\partial^2 u}{\partial k_x^2}\Big| u\Big\rangle \mathcal{J}_y^1$$

$$\mathcal{J}_y^p = \mathbb{J}_y^p - \sum_{n=1}^{p-1} C(p,n)\Big\langle \frac{\partial^n u}{\partial k_x^n}\Big| u\Big\rangle \mathcal{J}_y^{p-n}$$

$$\Rightarrow \mathbb{J}_y^p = \sum_{n=0}^{p} C(p,n)\Big\langle \frac{\partial^n u}{\partial k_x^n}\Big| u\Big\rangle \mathcal{J}_y^{p-n}$$

where $C(p,n)$ is the nth binomial coefficient of order p. The last step uses the fact that $\mathcal{J}_y^0 = \mathbb{J}_y^0 = 0$ to complete the lower limit of the sum. These $\mathbb{J}$ are structured like higher order forms of the Berry curvature. If one can also connect to even more general quantities that have the form

$$Tr[\Big[Px^mP, Py^nP\Big]]$$

then this could calculate the Chern analogue of the GMP algebra in terms of the coefficients of the non-linear response of a singe filled Chern band system. With the terms here, we express the response in a way that it may connect to the conditions put forth in [Roy14] to the electric response of the system.

3.A Explicit Derivation of $\mathcal{J}_y$

Here contains a formal and step by step proof of the formula for $\mathcal{J}_y^p$, shown in section 3.4. We will consider a general hybrid Wannier function without using the freedom of placing the unit cell at the origin and simplify later.

3.A.1 Preliminaries

We will use the formal definition of the position operator that is robust to use in periodic systems.

$$\hat{x} \equiv \lim_{\alpha \to 0} \frac{e^{i\alpha x} - 1}{i\alpha}$$

Proof:

$$\lim_{\alpha \to 0} \frac{e^{i\alpha x} - 1}{i\alpha} = \lim_{\alpha \to 0} \frac{1 + i\alpha x + \frac{1}{2!}(i\alpha x)^2 + \cdots - 1}{i\alpha} = \lim_{\alpha \to 0} x + \frac{1}{2!} i\alpha x^2 + \mathcal{O}(\alpha^2) = x + 0 + 0 + \ldots$$

Corollary:

$$i^p \hat{x}^p = \lim_{\alpha \to 0} \left(\frac{e^{i\alpha x} - 1}{\alpha} \right)^p$$

This can be seen by expanding out the right side in the same way and seeing that everything except the leading order in the Taylor series will have too many factors of α. In more than one dimension, a vector form is preferable for $\vec{\alpha} \equiv \alpha \hat{x}$

$$i^p x^p \equiv \lim_{|\vec{\alpha}| \to 0} \left(\frac{e^{i\vec{\alpha} \cdot \vec{r}} - 1}{|\vec{\alpha}|} \right)^p$$

3.A.2 Derivation

Starting with:

$$\langle P\hat{y}P\hat{x}^p P \rangle - \langle P\hat{x}^p P\hat{y}P \rangle = \langle \vec{R}, k_y, \alpha | P\hat{y}P\hat{x}^p P | \vec{R}, k_y, \alpha \rangle - \langle \vec{R}, k_y, \alpha | P\hat{x}^p P\hat{y}P | \vec{R}, k_y, \alpha \rangle$$

where $\vec{R}$ is a vector in the x direction with that being the localized direction of our hybrid Wannier states. Let us write P using the Bloch states $|\Psi_{\vec{k}}\rangle$ and then use the integral form

of our hybrid Wannier functions as presented in section 3.3.1

$$\int\int\int dk_x d^2\vec{k}' dk_x'' \langle \Psi_{\vec{k}} | e^{-ik_x R} \hat{y} | \Psi_{\vec{k}'} \rangle e^{ik_x' R} e^{-ik_x' R} \langle \Psi_{\vec{k}'} | \hat{x}^p e^{ik_x'' R} | \Psi_{\vec{k}''} \rangle$$

$$- \langle \Psi_{\vec{k}} | e^{-ik_x R} \hat{x}^p | \Psi_{\vec{k}'} \rangle e^{ik_x' R} e^{-ik_x' R} \langle \Psi_{\vec{k}'} | \hat{y} e^{ik_x'' R} | \Psi_{\vec{k}''} \rangle$$

We are free to add the exponentials in terms of k' as they multiply to 1. Next, we separate out our Bloch functions into $|\Psi_{\vec{k}}\rangle = e^{i\vec{k}\cdot\vec{r}}|U_k\rangle$.

$$\int\int\int dk_x d^2\vec{k}' dk_x'' \langle U_k | \hat{y} e^{i(\vec{k}-\vec{k}')\cdot(\hat{\vec{r}}-\vec{R})} | U_{k'} \rangle \langle U_{k'} | \hat{x}^p e^{i(\vec{k}'-\vec{k}'')\cdot(\hat{\vec{r}}-\vec{R})} | U_{\vec{k}''} \rangle$$

$$- \langle U_k | \hat{x}^p e^{i(\vec{k}-\vec{k}')\cdot(\hat{\vec{r}}-\vec{R})} | U_{k'} \rangle \langle U_{k'} | \hat{y} e^{i(\vec{k}'-\vec{k}'')\cdot(\hat{\vec{r}}-\vec{R})} | U_{\vec{k}''} \rangle$$

From this point, we need to make a shift in our coordinates to the unit cell R_x that the Wannier states are located within. We will also multiply through by factors of i to prepare to transform our position operators into derivatives.

$$i^{-(p+1)} \int\int\int dk_x d^2\vec{k}' dk_x'' \langle U_k | i\hat{y} e^{i(\vec{k}-\vec{k}')\cdot\hat{\vec{r}}} | U_{k'} \rangle \langle U_{k'} | (i\hat{x} + iR_x)^p e^{i(\vec{k}'-\vec{k}'')\cdot\hat{\vec{r}}} | U_{\vec{k}''} \rangle$$

$$- \langle U_k | (i\hat{x} + iR_x)^p e^{i(\vec{k}-\vec{k}')\cdot\hat{\vec{r}}} | U_{k'} \rangle \langle U_{k'} | i\hat{y} e^{i(\vec{k}'-\vec{k}'')\cdot\hat{\vec{r}}} | U_{\vec{k}''} \rangle$$

For this next transformation, we will consider only the leading x^p term in $i^{-p}(i\hat{x} + iR_x)^p$ to show the derivative formalism works in general, then we will come back at the end and fill in. As we substitute our limit forms of x and y using $\vec{\alpha} = \alpha\hat{e_x}$ and $\vec{\beta} = \beta\hat{e_y}$, note that the form of $\hat{x}^p$ is expanded in terms of binomial coefficients $\binom{m}{n}$

$$\lim_{|\alpha|,|\beta|\to 0} \frac{1}{i^{p+1}|\alpha|^p|\beta|} \int\int\int dk_x d^2\vec{k}' dk_x''$$

$$\langle U_k | (e^{i\vec{\beta}\cdot\vec{r}} - 1) e^{i(\vec{k}-\vec{k}')\cdot\vec{r}} | U_{k'} \rangle \times$$

$$\langle U_{k'} | (e^{pi\vec{\alpha}\cdot\vec{r}} - \tbinom{p}{1} e^{(p-1)i\vec{\alpha}\cdot\vec{r}} + \tbinom{p}{2} e^{(p-2)i\vec{\alpha}\cdot\vec{r}} - \cdots - 1) e^{i(\vec{k}'-\vec{k}'')\cdot\vec{r}} | U_{\vec{k}''} \rangle$$

$$- \langle U_k | (e^{pi\vec{\alpha}\cdot\vec{r}} - \tbinom{p}{1} e^{(p-1)i\vec{\alpha}\cdot\vec{r}} + \tbinom{p}{2} e^{(p-2)i\vec{\alpha}\cdot\vec{r}} - \cdots - 1) e^{i(\vec{k}-\vec{k}')\cdot\vec{r}} | U_{k'} \rangle \times$$

$$\langle U_{k'} | (e^{i\vec{\beta}\cdot\vec{r}} - 1) e^{i(\vec{k}'-\vec{k}'')\cdot\vec{r}} | U_{\vec{k}''} \rangle$$

$$=$$

$$\lim_{|\alpha|,|\beta|\to 0} \frac{1}{i^{p+1}|\alpha|^p|\beta|} \int\int\int dk_x d^2\vec{k}' dk_x''$$
$$\langle U_k|(e^{i(\vec{k}'-\vec{k}+\vec{\beta})\cdot\vec{r}} - e^{i(\vec{k}'-\vec{k})\cdot\vec{r}})|U_{k'}\rangle\langle U_{k'}|(e^{i(\vec{k}''-\vec{k}'+p\vec{\alpha})\cdot\vec{r}} - \cdots - e^{i(\vec{k}''-\vec{k}')\cdot\vec{r}})|U_{k''}\rangle$$
$$- \langle U_k|(e^{i(\vec{k}'-\vec{k}+p\vec{\alpha})\cdot\vec{r}} - \cdots - e^{i(\vec{k}'-\vec{k})\cdot\vec{r}})|U_{k'}\rangle\langle U_{k'}|(e^{i(\vec{k}''-\vec{k}'+\vec{\beta})\cdot\vec{r}} - e^{i(\vec{k}''-\vec{k}')\cdot\vec{r}})|U_{k''}\rangle$$

Here, term by term, we can make a shift of variable in $\vec{k}'$ and then $\vec{k}''$ to absorb β and α into the periodic part of the Bloch function

$$\lim_{|\alpha|,|\beta|\to 0} \frac{1}{i^{p+1}|\alpha|^p|\beta|} \int\int\int dk_x d^2\vec{k}' dk_x''$$
$$\langle U_k|e^{i(\vec{k}'-\vec{k})\cdot\vec{r}}\Big(|U_{k'-\vec{\beta}}\rangle\langle U_{k'-\vec{\beta}}|(e^{i(\vec{k}''-\vec{k}'+p\vec{\alpha}+\vec{\beta})\cdot\vec{r}} - \cdots - e^{i(\vec{k}''-\vec{k}'+\vec{\beta})\cdot\vec{r}})|U_{k''}\rangle$$
$$- |U_{k'}\rangle\langle U_{k'}|(e^{i(\vec{k}''-\vec{k}'+p\vec{\alpha})\cdot\vec{r}} - \cdots - e^{i(\vec{k}''-\vec{k}')\cdot\vec{r}})|U_{k''}\rangle\Big)$$
$$- \langle U_k|e^{i(\vec{k}'-\vec{k})\cdot\vec{r}}\Big(|U_{k'-p\vec{\alpha}}\rangle\langle U_{k'-p\vec{\alpha}}|(e^{i(\vec{k}''-\vec{k}'+p\vec{\alpha}+\vec{\beta})\cdot\vec{r}} - e^{i(\vec{k}''-\vec{k}'+p\vec{\alpha})\cdot\vec{r}})|U_{k''}\rangle$$
$$- \cdots - |U_{k'}\rangle\langle U_{k'}|(e^{i(\vec{k}''-\vec{k}'-\vec{\beta})\cdot\vec{r}} - e^{i(\vec{k}''-\vec{k}')\cdot\vec{r}})|U_{k''}\rangle\Big)$$

$$=$$

$$\lim_{|\alpha|,|\beta|\to 0} \frac{1}{i^{p+1}|\alpha|^p|\beta|} \int\int\int dk_x d^2\vec{k}' dk_x''$$
$$\langle U_k|e^{i(\vec{k}'-\vec{k})\cdot\vec{r}}\Big(|U_{k'-\vec{\beta}}\rangle\langle U_{k'-\vec{\beta}}|e^{i(\vec{k}''-\vec{k}')\cdot\vec{r}}|(|U_{k''-p\vec{\alpha}-\vec{\beta}}\rangle - \cdots - |U_{k''-\vec{\beta}}\rangle)$$
$$- |U_{k'}\rangle\langle U_{k'}|e^{i(\vec{k}''-\vec{k}')\cdot\vec{r}}(|U_{k''-p\vec{\alpha}}\rangle - \cdots - |U_{k''}\rangle)\Big)$$
$$- \langle U_k|e^{i(\vec{k}'-\vec{k})\cdot\vec{r}}\Big(|U_{k'-p\vec{\alpha}}\rangle\langle U_{k'-p\vec{\alpha}}|e^{i(\vec{k}''-\vec{k}')\cdot\vec{r}}(|U_{k''-p\vec{\alpha}-\vec{\beta}}\rangle - |U_{k''-p\vec{\alpha}}\rangle)$$
$$- \cdots - |U_{k'}\rangle\langle U_{k'}|e^{i(\vec{k}''-\vec{k}')\cdot\vec{r}}(|U_{k''-\vec{\beta}}\rangle - |U_{k''}\rangle)\Big)$$

Due to the infinitesimal nature of α and β, these inner products between U_k states are approximately diagonal and therefore, in the limit, k, k', k'' must all be equal. This simplifies from 3 to only 1 integral and forces the exponentials to unity. This is equivalent to identifying the integral form of the delta function here. Then, noting that the limit form of the p^{th} derivative is

$$\frac{\partial^p f}{\partial \vec{k}_{\hat{n}}^p} = \lim_{|\gamma|\to 0} \frac{f(\vec{k}+p\vec{\gamma}) - \binom{p}{1} f(\vec{k}+(p-1)\vec{\gamma}) + \cdots - f(\vec{k})}{|\gamma|^p}$$

where $\hat{n} = \frac{\vec{\gamma}}{|\gamma|}$ and $\vec{k}_{\hat{n}} = (\vec{k} \cdot \hat{n})\hat{n}$, we can make the substitution of $\alpha \to -\alpha$ and $\beta \to -\beta$ without changing the overall sign and evaluate the α limit and then the β limit to get derivatives in U.

$$i^{-(p+1)} \int dk_x \langle U_k | \frac{\partial}{\partial \vec{k}_y} \Big(|U_k\rangle \Big\langle U_k \Big| \frac{\partial^p U_k}{\partial \vec{k}_x^p} \Big\rangle \Big) - \langle U_k | \frac{\partial^p}{\partial \vec{k}_x^p} \Big(|U_k\rangle \Big\langle U_k \Big| \frac{\partial U_k}{\partial \vec{k}_y} \Big\rangle \Big)$$

Now reintroduce iR_x from the original calculation.

$$i^{-(p+1)} \int dk_x \langle U_k | \frac{\partial}{\partial \vec{k}_y} \Big(|U_k\rangle \langle U_k | (\frac{\partial}{\partial \vec{k}_x} + iR_x)^p |U_k\rangle \Big) - \langle U_k | (\frac{\partial}{\partial \vec{k}_x} + iR_x)^p \Big(|U_k\rangle \langle U_k | \frac{\partial}{\partial \vec{k}_y} |U_k\rangle \Big)$$

where choosing R_x to be zero gives the formula for $\mathcal{J}_y^p$ that we state in section 3.4. Keeping the factor of R_x through the calculation of these expressions may have use in calculations that wish to compare multiple unit cells, but is not necessary here.

3.B Calculation of $\mathcal{J}_y^p$ for $p = 2, 3$ for a general Chern insulator

Here we calculate the first few terms of $\mathcal{J}_y^p$ that were used to find the recursive relations in terms of existing band geometric quantities.

3.B.1 $p = 2$ term in terms of geometric quantities

Starting from

$$-i \int dk_x \langle U_k | \frac{\partial}{\partial \vec{k}_y} \Big(|U_k\rangle \langle U_k | (\frac{\partial}{\partial \vec{k}_x} + iR_x)^2 |U_k\rangle \Big) - \langle U_k | (\frac{\partial}{\partial \vec{k}_x} + iR_x)^2 \Big(|U_k\rangle \langle U_k | \frac{\partial}{\partial \vec{k}_y} |U_k\rangle \Big)$$

we can act the outermost derivatives and cancel a few terms as so

$$-i \int dk_x \langle U_k | \frac{\partial}{\partial \vec{k}_y} |U_k\rangle \langle U_k | (\frac{\partial}{\partial \vec{k}_x} + iR_x)^2 |U_k\rangle + \langle U_k | \frac{\partial^\dagger}{\partial \vec{k}_y} (\frac{\partial}{\partial \vec{k}_x} + iR_x)^2 |U_k\rangle$$

$$+ \langle U_k | \frac{\partial}{\partial \vec{k}_y} (\frac{\partial}{\partial \vec{k}_x} + iR_x)^2 |U_k\rangle - \langle U_k | (\frac{\partial}{\partial \vec{k}_x} + iR_x)^2 \frac{\partial}{\partial \vec{k}_y} |U_k\rangle - 2iR_x \langle U_k | \frac{\partial}{\partial \vec{k}_x} \Big(|U_k\rangle \langle U_k| \Big) \frac{\partial}{\partial \vec{k}_y} |U_k\rangle$$

$$- \langle U_k | \frac{\partial^2}{\partial \vec{k}_x^2} \Big(|U_k\rangle \langle U_k| \Big) \frac{\partial}{\partial \vec{k}_y} |U_k\rangle - 2 \langle U_k | \frac{\partial}{\partial \vec{k}_x} \Big(|U_k\rangle \langle U_k| \Big) \frac{\partial}{\partial \vec{k}_x} \frac{\partial}{\partial \vec{k}_y} |U_k\rangle$$

The 3rd and 4th term cancel. We can expand the quadratic derivative factors for more cancellations

$$-i\int dk_x\langle U_k|\frac{\partial}{\partial\vec{k}_y}|U_k\rangle\langle U_k|\frac{\partial^2}{\partial\vec{k}_x^2}|U_k\rangle + 2iR_x\langle U_k|\frac{\partial}{\partial\vec{k}_y}|U_k\rangle\langle U_k|\frac{\partial}{\partial\vec{k}_x}|U_k\rangle - R_x^2\langle U_k|\frac{\partial}{\partial\vec{k}_y}|U_k\rangle$$

$$+\langle U_k|\frac{\partial^\dagger}{\partial\vec{k}_y}\frac{\partial^2}{\partial\vec{k}_x^2}|U_k\rangle + 2iR_x\langle U_k|\frac{\partial^\dagger}{\partial\vec{k}_y}\frac{\partial}{\partial\vec{k}_x}|U_k\rangle - R_x^2\langle U_k|\frac{\partial^\dagger}{\partial\vec{k}_y}|U_k\rangle$$

$$-2iR_x\langle U_k|\frac{\partial}{\partial\vec{k}_x}|U_k\rangle\langle U_k|\frac{\partial}{\partial\vec{k}_y}|U_k\rangle - 2iR_x\langle U_k|\frac{\partial^\dagger}{\partial\vec{k}_x}\frac{\partial}{\partial\vec{k}_y}|U_k\rangle$$

$$-\langle U_k|\frac{\partial^2}{\partial\vec{k}_x^2}|U_k\rangle\langle U_k|\frac{\partial}{\partial\vec{k}_y}|U_k\rangle - \langle U_k|\frac{\partial^{\dagger 2}}{\partial\vec{k}_x^2}\frac{\partial}{\partial\vec{k}_y}|U_k\rangle - 2\langle U_k|\frac{\partial}{\partial\vec{k}_x}|U_k\rangle\langle U_k|\frac{\partial^\dagger}{\partial\vec{k}_x}\frac{\partial}{\partial\vec{k}_y}|U_k\rangle$$

$$-2\langle U_k|\frac{\partial}{\partial\vec{k}_x}|U_k\rangle\langle U_k|\frac{\partial}{\partial\vec{k}_x}\frac{\partial}{\partial\vec{k}_y}|U_k\rangle - 2\langle U_k|\frac{\partial^\dagger}{\partial\vec{k}_x}\frac{\partial}{\partial\vec{k}_x}\frac{\partial}{\partial\vec{k}_y}|U_k\rangle$$

Here, the 1st term on the 1st and 4th lines cancel, the last term on the 1st and 2nd lines combine to be $-R_x^2\frac{\partial}{\partial\vec{k}_y}\langle U_k|U_k\rangle$ which is zero as it is a derivative of a constant. The 2nd term on the 1st line and the 1st term on the 3rd line cancel. Rearranging the remaining terms we get

$$-i\int dk_x 2iR_x\langle U_k|\frac{\partial^\dagger}{\partial\vec{k}_y}\frac{\partial}{\partial\vec{k}_x}|U_k\rangle - 2iR_x\langle U_k|\frac{\partial^\dagger}{\partial\vec{k}_x}\frac{\partial}{\partial\vec{k}_y}|U_k\rangle$$

$$+\langle U_k|\frac{\partial^\dagger}{\partial\vec{k}_y}\frac{\partial^2}{\partial\vec{k}_x^2}|U_k\rangle - \langle U_k|\frac{\partial^{\dagger 2}}{\partial\vec{k}_x^2}\frac{\partial}{\partial\vec{k}_y}|U_k\rangle - 2\langle U_k|\frac{\partial}{\partial\vec{k}_x}|U_k\rangle\langle U_k|\frac{\partial^\dagger}{\partial\vec{k}_x}\frac{\partial}{\partial\vec{k}_y}|U_k\rangle$$

$$-2\langle U_k|\frac{\partial}{\partial\vec{k}_x}|U_k\rangle\langle U_k|\frac{\partial}{\partial\vec{k}_x}\frac{\partial}{\partial\vec{k}_y}|U_k\rangle - 2\langle U_k|\frac{\partial^\dagger}{\partial\vec{k}_x}\frac{\partial}{\partial\vec{k}_x}\frac{\partial}{\partial\vec{k}_y}|U_k\rangle$$

We then see that we can pull out the Berry curvature $\mathcal{F}$ in multiple places. The first line is just in the right form and the 2nd and 3rd line require adding zero to pull out an overall derivative in k_x

$$-i\int dk_x 2iR_x\mathcal{F} + \frac{\partial}{\partial\vec{k}_x}\Big(\langle U_k|\frac{\partial^\dagger}{\partial\vec{k}_y}\frac{\partial}{\partial\vec{k}_x}|U_k\rangle - \langle U_k|\frac{\partial^\dagger}{\partial\vec{k}_x}\frac{\partial}{\partial\vec{k}_y}|U_k\rangle\Big)$$

$$-\langle U_k|\frac{\partial^\dagger}{\partial\vec{k}_y}\frac{\partial^\dagger}{\partial\vec{k}_x}\frac{\partial}{\partial\vec{k}_x}|U_k\rangle - \langle U_k|\frac{\partial^\dagger}{\partial\vec{k}_x}\frac{\partial}{\partial\vec{k}_x}\frac{\partial}{\partial\vec{k}_y}|U_k\rangle$$

$$-2\langle U_k|\frac{\partial}{\partial\vec{k}_x}|U_k\rangle\langle U_k|\frac{\partial}{\partial\vec{k}_x}\frac{\partial}{\partial\vec{k}_y}|U_k\rangle - 2\langle U_k|\frac{\partial}{\partial\vec{k}_x}|U_k\rangle\langle U_k|\frac{\partial^\dagger}{\partial\vec{k}_x}\frac{\partial}{\partial\vec{k}_y}|U_k\rangle$$

We can rewrite the 2nd line by pulling out a derivative of k_y and we can add zero to the 3rd line, to de the same to the 1st term. Then we find the pair for the 2nd term to become the Berry Curvature

$$-i\int dk_x 2iR_x\mathcal{F}+\frac{\partial}{\partial\vec{k}_x}\mathcal{F}$$
$$-\frac{\partial}{\partial\vec{k}_y}\langle U_k|\frac{\partial^\dagger}{\partial\vec{k}_x}\frac{\partial}{\partial\vec{k}_x}|U_k\rangle$$
$$-2\langle U_k|\frac{\partial}{\partial\vec{k}_x}|U_k\rangle\frac{\partial}{\partial\vec{k}_y}\langle U_k|\frac{\partial}{\partial\vec{k}_x}|U_k\rangle+2\mathcal{F}\langle U_k|\frac{\partial}{\partial\vec{k}_x}|U_k\rangle$$

The 1st term on the 3rd line is also a total derivative of a square, se we can rearrange the terms to simplify further.

$$-i\int dk_x\Big(2\langle U_k|\frac{\partial}{\partial\vec{k}_x}|U_k\rangle+2iR_x+\frac{\partial}{\partial\vec{k}_x}\Big)\mathcal{F}$$
$$-\frac{\partial}{\partial\vec{k}_y}\Big(\langle U_k|\frac{\partial^\dagger}{\partial\vec{k}_x}\frac{\partial}{\partial\vec{k}_x}|U_k\rangle+\langle U_k|\frac{\partial}{\partial\vec{k}_x}|U_k\rangle\langle U_k|\frac{\partial}{\partial\vec{k}_x}|U_k\rangle\Big)$$

Finally the term on the 2nd line can now be recognized as the k_y derivative of the diagonal part of the quantum metric, afterward denoted as g_{xx}. Also on the first line we see the x component of the Berry connection which will be denoted as $-iA_x$.

$$-i\int dk_x\Big(2A_x+2iR_x+\frac{\partial}{\partial\vec{k}_x}\Big)\mathcal{F}-\frac{\partial}{\partial\vec{k}_y}g_{xx}$$

In the Landau level, this term vanishes. The metric is flat and R_x can be seen as the center of the harmonic oscillator part of the wave function and cancel with A_x. Then we are left with a boundary term for $\mathcal{F}$ which is zero as the Berry curvature must be smoothly periodic within the Brillouin zone. In fact, in any case we wish to consider, we see that any sort of k_x derivative term will vanish due to the fact that it is under an integral over k_x as we are guaranteed smooth periodicity on the wavefunctions. The flatness of the metric, however is not generically true, so there would be contributions to this order in general from that term.

3.B.2 $p = 3$ term in terms of geometric quantities

Now that we understand the simplification process, we will skip the cancellation and show our answer in terms of band geometric quantities.

$$\int dk_x \langle U_k| \frac{\partial}{\partial \vec{k}_y} \Big(|U_k\rangle\langle U_k| (\frac{\partial}{\partial \vec{k}_x} + iR_x)^3 |U_k\rangle \Big) - \langle U_k| (\frac{\partial}{\partial \vec{k}_x} + iR_x)^3 \Big(|U_k\rangle\langle U_k| \frac{\partial}{\partial \vec{k}_y} |U_k\rangle \Big)$$

$$=$$

$$\int dk_x \frac{\partial^2}{\partial \vec{k}_x^2}\mathcal{F} - 3i\frac{\partial}{\partial \vec{k}_x}\Big[(A_x - R_x)\mathcal{F}\Big] - 3(A_x - R_x)^2\mathcal{F} - 6g_{xx}\mathcal{F}$$
$$+ 3i(A_x - R_x)\frac{\partial}{\partial \vec{k}_y} g_{xx} + \frac{\partial}{\partial \vec{k}_y}\Big[G_{xxx} - \frac{\partial}{\partial \vec{k}_x} g_{xx}\Big]$$

Where G_{xxx} is a band geometric quantity of a similar form to the metric

$$G_{xxx} = Tr[PxQxQxP] = 2(\langle U_k| \frac{\partial}{\partial \vec{k}_x} |U_k\rangle)^3 \; - \langle U_k| \frac{\partial^2}{\partial \vec{k}_x^2} |U_k\rangle\langle U_k| \frac{\partial}{\partial \vec{k}_x} |U_k\rangle$$
$$- \langle U_k| \frac{\partial^\dagger}{\partial \vec{k}_x} \frac{\partial^2}{\partial \vec{k}_x^2} |U_k\rangle + 2\langle U_k| \frac{\partial}{\partial \vec{k}_x} |U_k\rangle\langle U_k| \frac{\partial^\dagger}{\partial \vec{k}_x} \frac{\partial}{\partial \vec{k}_x} |U_k\rangle$$

Much like before we can impose continuity of the Brillouin zone boundary conditions to remove terms from J_y^3 which don't contribute to the current per hybrid Wannier orbital

$$\langle \hat{j}_y \rangle^{(p)} = \int dk_x \left[-3(A_x - R_x)^2\mathcal{F} - 6g_{xx}\mathcal{F} + 3i(A_x - R_x)\frac{\partial}{\partial \vec{k}_y} g_{xx} + \frac{\partial}{\partial \vec{k}_y} G_{xxx} \right]$$

Within the Landau level this simplifies to the expression given in [Bis13] with the Hall viscosity terms coming from the first two terms containing the Berry curvature. Perturbatively, using the $1/N$ expansion of small flux within the Hofstadter model, we can write the Bloch periodic wavefunctions as

$$|U_k\rangle_{Hof} = U(a, a^\dagger)|U_k\rangle_{LL} = e^{f(a,a^\dagger)}|U_k\rangle_{LL}$$

with

$$f(a, a^\dagger) = -\frac{\pi}{96N}(a^{\dagger 4} - a^4) - \frac{\pi^2}{N^2}(\frac{1}{128}a^{\dagger 4} + \frac{1}{320}a^{\dagger 5}a - H.c.)$$

Given this we can find that the effect on the order $p = 2$ is still zero. The effect at $p = 3$ to order $1/N^2$ in the nth filled Hofstadter band is

$$\frac{3\pi^2}{144N^2} l_B^4 (n + \frac{1}{2})(n^2 + n + 3)$$

which is consistent with the results found in [HBJ18].

3.B.3 Relating $\mathcal{J}_y^p$ and $\mathbb{J}_y^p$

Given the forms obtained in the previous sections, we can show how $\mathcal{J}_y^p$ relates to the gauge independent geometric quantities $\mathbb{J}_y^p$. Remembering the definition of $\mathbb{J}_y^p$ and

$$\mathbb{J}_y^m \equiv Tr\Big[[P_\alpha \frac{\partial}{\partial \vec{k}_y} P_\alpha, P_\alpha \frac{\partial^m}{\partial \vec{k}_x^m} P_\alpha]\Big]$$

It's easy to see that it is just the Berry curvature

$$\mathbb{J}_y^1 = \mathcal{J}_y^1 = \mathcal{F}$$

This is not surprising as the first order would just be the response if we had a constant electric field.

Now, consider the next two terms using the fact that $A_x = \langle \partial_{k_x} \rangle = -\langle \partial_{k_x}^\dagger \rangle$

$$\mathbb{J}_y^2 = \mathcal{J}_y^2 + 2\langle \partial_{k_x}^\dagger \rangle \mathcal{J}_y^1 = \frac{\partial \mathcal{F}}{\partial \vec{k}_x} + \frac{\partial g_{xx}}{\partial \vec{k}_y}$$

$$\mathbb{J}_y^3 = \mathcal{J}_y^3 + 3\langle \partial_{k_x}^\dagger \rangle \mathcal{J}_y^2 + 3\langle \partial_{k_x}^{\dagger 2} \rangle \mathcal{J}_y^1$$

We notice that the difference between $\mathbb{J}_y^3$ and $\mathcal{J}_y^3$ comes from the extra action of the k_x derivatives on the rightmost projector due to the cyclic periodicity of the trace. It is given this understanding that allows us to generalize the relation as

$$\mathbb{J}_y^p = \sum_{n=0}^{p} C(p,n) \Big\langle \frac{\partial^n u}{\partial k_x^n} \Big| u \Big\rangle \mathcal{J}_y^{p-n}$$

CHAPTER 4

Floquet Topological Phases

4.1 Introduction to Periodically Driven Systems

It is important for the following research that we review topologically time dependent systems. Given a time dependent Hamiltonian $H(t)$, the unitary evolution operator is defined as so

$$U(t) = \mathcal{T} \exp\left[-i \int_0^t H(t')dt' \right]$$

where $\mathcal{T}$ denotes the time ordering operator. The rigorous expression of the exponential of this exponentiated integral of a Hamiltonian is one of a Taylor series, so we need to make sure that the integrals are evaluated in a causal way. The explicit form of $\mathcal{T}$ for two operators $V_1(t_1), V_2(t_2)$ is

$$\mathcal{T}\big[V_1(t_1)V_2(t_2)\big] = \Theta(t_1 - t_2)V_1(t_1)V_2(t_2) + \Theta(t_2 - t_1)V_2(t_2)V_1(t_1)$$

where $\Theta(t)$ is the Heaviside step operator.

If the Hamiltonian is time periodic, $H(t+T) = H(t)$, for some period T, then our unitary is not guaranteed to be periodic. To study a time periodic system, instead of looking at the spectrum of the Hamiltonian as in a static system, we look at the spectrum of the unitary operator. Particularly, the unitary after one whole evolution, $U(T)$, can be written in the eigenspace of the unitary, $|\phi_n(t)\rangle$, as

$$U(T)|\phi_n(0)\rangle = e^{-i\epsilon_n T}|\phi_n(0)\rangle$$

which is an analogue of Bloch's theorem. The values, ϵ_n, are known as quasienergies and can only be defined modulo $2\pi/T$. One would then be interested in defining a static Hamiltonian,

H_F, whose eigenvalues on the set $\{|\phi_n(T)\rangle\}$ are $\{\epsilon_n\}$, such that

$$H_F = \frac{i}{T} \ln U(T) \Rightarrow e^{-iH_F T} = U(T)$$

however, one must be careful. The spectrum of ϵ_n must be gapped at a quasienergy or else the logarithm, and therefore H_F, does not have a well defined branch cut. However, the choice of branch cut must also respect the symmetries of $H(t)$, like particle/hole or chiral symmetry which both swap upper and lower bands. This generally means a choice of branch cut at $\pi, -\pi$. If we can do this in a well defined way, we call H_F the Floquet Hamiltonian. Note that it is possible to find such band configuration to define an equivalent static Hamiltonian for $U(t)$ anywhere during the evolution, but the eigenstates will we different than at $t = 0$ or T.

4.2 The Loop Formalism

It is useful for our analysis to be able to consider periodic unitaries such that

$$U(T) = U(0) = \mathbb{1}$$

where setting $U(0)$ to the identity can be done without loss of generality by prepending a Hamiltonian to the evolution that exponentiates to $U(0)^{-1}$. However, it shouldn't be assumed that a general unitary evolution, even of a periodic Hamiltonian, has this property. As we saw earlier, generally there may be a spectrum of quasienergies with one period of evolution being free to give each eigenstate its own phase. Indeed, our definition of the Floquet Hamiltonian gives the difference between the beginning and end of the evolution. As will be demonstrated below, we can use this to always deconstruct an arbitrary unitary evolution into a loop part and a constant part using the Floquet Hamiltonian that still respects the underlying symmetries of $H(t)$, via a construction further detailed in ref [RH17].

As we will consider a chiral symmetric system later, we will look at an example of this construction using a Hamiltonian with only chiral symmetry. The statement of chiral

symmetry requires any new Hamiltonian we construct to obey

$$CH(\vec{k})C^{-1} = -H(\vec{k})$$

but because of our construction of the Floquet Hamiltonian, it inherently respects the symmetries of the Hamiltonian. Additionally, by writing our Floquet Hamiltonian in terms of the eigensystem of our unitary, it was shown that this construction gives us a local operator[GT18]. Therefore, our exponentiated Floquet Hamiltonian is a local operator that respects the symmetry of our system so we can homotopically deform our system to a loop by defining a new Hamiltonian via H_F.

$$H_L(t) = \begin{cases} -2H_F & 0 \leq t < \frac{1}{4}T \\ 2H(2(t - \frac{1}{4}T)) & \frac{1}{4}T \leq t < \frac{3}{4}T \\ -2H_F & \frac{3}{4}T \leq t < T \end{cases}$$

We have taken our original evolution and added evolutions by H_F on either side of half the constant Floquet Hamiltonian evolution, $\exp\{-iH_FT/2\}$, then rescaled everything so that we have the same period. The unitary evolution of our new Hamiltonian is now a loop. Our original evolution can be seen as equivalent to the evolution around the corresponding loop we have constructed and a constant evolution of the Floquet Hamiltonian. The constant Floquet Hamiltonian cannot contain any dynamical topological properties (as it is constant and does not close the gap) so our dynamical properties of our unitary evolution are the same as the properties of the loop. For our research we will only consider the dynamical properties of loops and this equivalency shows that this will be sufficient to see the properties of the corresponding class of unitary evolutions.

4.3 The Floquet Periodic Table

Our motivation for studying Floquet systems comes from the recent classification of Floquet topological phases that mirrors the result for static topological insulators discussed earlier. We can classify our unitaries into Altland-Zirnbauer classes by the symmetry of the time dependent Hamiltonian.

class	Θ	P	C	d=0	1	2	3	4	5	6	7
A				$\mathbb{Z}\times\mathbb{Z}$	$\emptyset$	$\mathbb{Z}\times\mathbb{Z}$	$\emptyset$	$\mathbb{Z}\times\mathbb{Z}$	$\emptyset$	$\mathbb{Z}\times\mathbb{Z}$	$\emptyset$
AIII			1	$\emptyset$	$\mathbb{Z}\times\mathbb{Z}$	$\emptyset$	$\mathbb{Z}\times\mathbb{Z}$	$\emptyset$	$\mathbb{Z}\times\mathbb{Z}$	$\emptyset$	$\mathbb{Z}\times\mathbb{Z}$
AI	+1			$\mathbb{Z}\times\mathbb{Z}$	$\emptyset$	$\emptyset$	$\emptyset$	$\mathbb{Z}\times\mathbb{Z}$	$\emptyset$	$\mathbb{Z}_2\times\mathbb{Z}_2$	$\mathbb{Z}_2\times\mathbb{Z}_2$
BDI	+1	+1	1	$\mathbb{Z}_2\times\mathbb{Z}_2$	$\mathbb{Z}\times\mathbb{Z}$	$\emptyset$	$\emptyset$	$\emptyset$	$\mathbb{Z}\times\mathbb{Z}$	$\emptyset$	$\mathbb{Z}_2\times\mathbb{Z}_2$
D		+1		$\mathbb{Z}_2\times\mathbb{Z}_2$	$\mathbb{Z}_2\times\mathbb{Z}_2$	$\mathbb{Z}\times\mathbb{Z}$	$\emptyset$	$\emptyset$	$\emptyset$	$\mathbb{Z}\times\mathbb{Z}$	$\emptyset$
DIII	-1	+1	1	$\emptyset$	$\mathbb{Z}_2\times\mathbb{Z}_2$	$\mathbb{Z}_2\times\mathbb{Z}_2$	$\mathbb{Z}\times\mathbb{Z}$	$\emptyset$	$\emptyset$	$\emptyset$	$\mathbb{Z}\times\mathbb{Z}$
AII	-1			$\mathbb{Z}\times\mathbb{Z}$	$\emptyset$	$\mathbb{Z}_2\times\mathbb{Z}_2$	$\mathbb{Z}_2\times\mathbb{Z}_2$	$\mathbb{Z}\times\mathbb{Z}$	$\emptyset$	$\emptyset$	$\emptyset$
CII	-1	-1	1	$\emptyset$	$\mathbb{Z}\times\mathbb{Z}$	$\emptyset$	$\mathbb{Z}_2\times\mathbb{Z}_2$	$\mathbb{Z}_2\times\mathbb{Z}_2$	$\mathbb{Z}\times\mathbb{Z}$	$\emptyset$	$\emptyset$
C		-1		$\emptyset$	$\emptyset$	$\mathbb{Z}\times\mathbb{Z}$	$\emptyset$	$\mathbb{Z}_2\times\mathbb{Z}_2$	$\mathbb{Z}_2\times\mathbb{Z}_2$	$\mathbb{Z}\times\mathbb{Z}$	$\emptyset$
CI	+1	-1	1	$\emptyset$	$\emptyset$	$\emptyset$	$\mathbb{Z}\times\mathbb{Z}$	$\emptyset$	$\mathbb{Z}_2\times\mathbb{Z}_2$	$\mathbb{Z}_2\times\mathbb{Z}_2$	$\mathbb{Z}\times\mathbb{Z}$

Table 4.1: The periodic classification of topological phases and mirrors the static case. Here each nontrivial phase has two indices, and again for $d \geq 8$ the pattern repeats as dictated by Bott periodicity[Bot59].

The actions of the symmetries have a slightly different form when considered on unitaries. Time reversal symmetry has the additional mapping of $t \to T - t$ that has to be considered. Additionally, we use the Taylor expansion of the integral of the unitary to see that conjugation of the unitary and the Hamiltonian are equivalent

$$\begin{aligned}
&\mathcal{T}\exp\left[-i\int_0^t \mathcal{O}H(t')\mathcal{O}^{-1}dt'\right] \\
&= \mathcal{T}\left[1 - i\mathcal{O}\int_0^t H(t')dt'\mathcal{O}^{-1} - \mathcal{O}\int_0^t H(t')dt'\mathcal{O}^{-1}\mathcal{O}\int_0^t H(t'')dt''\mathcal{O}^{-1} + \ldots\right] \\
&= \mathcal{T}\mathcal{O}\exp\left[-i\int_0^t H(t')dt'\right]\mathcal{O}^{-1} \\
&= \mathcal{O}U(t)\mathcal{O}^{-1}
\end{aligned}$$

Therefore we can write down the effect of the symmetries on the unitary evolution

$$\Theta U(\vec{k},t)\Theta^{-1} = U^*(-\vec{k},T-t)U^T(-\vec{k},T)$$
$$PU(\vec{k},t)P^{-1} = U^*(-\vec{k},t)$$
$$CU(\vec{k},t)C^{-1} = -U(\vec{k},T-t)U^\dagger(\vec{k},T)$$

Using similar K-theory techniques as Kitaev, we can come up with a periodic table that classifies Floquet insulators (table 4.1)[RH17]. Comparing the two classifications, we see that the Floquet phases are classified by two invariants. These correspond to the static and dynamical components that we have already separated in our loop formalism. Indeed, the periodic table of static topological insulators just corresponds to the choice of trivial dynamical invariant for every system. In this way, the static periodic table is contained within the Floquet one.

4.4 1D Chiral Floquet Evolution

This section will show the concepts introduced here by considering an example system from ref [LHR18]. The model considered here is that of a bipartite 1D single particle chain with open boundary conditions and is shown schematically in fig 4.1. The chain has a number of unit cells N each with A and B sublattice sites.

The evolution is comprised of two static Hamiltonians, evolved in sequence. The Hamiltonians are

$$H_1 = \frac{2\pi}{T}\sum_i a_i^\dagger b_i + b_i^\dagger a_i$$
$$H_2 = \frac{2\pi}{T}\sum_i a_{i+1}^\dagger b_i + b_i^\dagger a_{i+1}$$

where $a_i^\dagger, a_i$ and $b_i^\dagger, b_i$ are the creation and annihilation operators for A and B sites in unit cell i. This model is based on the static Su-Schrieffer-Heeger (SSH) model [SSH79] which combines the H_1 and H_2 each with different couplings into a single Hamiltonian. For the static SSH Hamiltonian, if the coupling to H_1 (the hop within the cell) is stronger, the system is trivial. If the hopping between cells is stronger (H_2), then the system is topological.

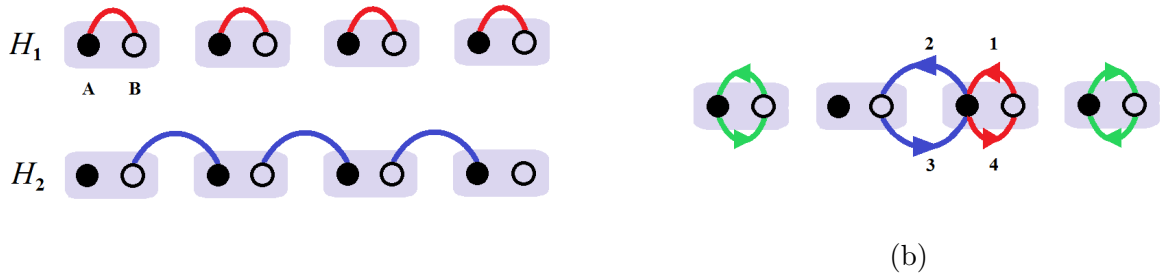

(a) (b)

Figure 4.1: The schematic picture of our Floquet evolution. 4.1a The two driving Hamiltonians we use. The filled (open) circles denote A (B) sites. Our trivial driving Hamiltonian, H_1, connects A and B sites in a single unit cell while the non-trivial H_2 connects adjacent unit cells. 4.1b The particles in the bulk of the chain move in closed trajectories, returning to their initial site unchanged. The particles at the boundaries are also mapped onto themselves but pick up a phase of π.

The unitary for the Floquet chiral chain comes from a sequential combination of the two Hamiltonians.

$$H(t) = \begin{cases} H_1 & 0 \leq t < \frac{1}{4}T \\ H_2 & \frac{1}{4}T \leq t < \frac{1}{2}T \\ H_2 & \frac{1}{2}T \leq t < \frac{3}{4}T \\ H_1 & \frac{3}{4}T \leq t < T \end{cases}$$

Due to having static Hamiltonians at each step, we can think of the unitaries of each step of the drive individually. As each Hamiltonian is a σ_x operator between two sites, exponentiating it we can write the unitary within the basis of two connected sites for step i as

$$U_i(t) = \begin{pmatrix} \cos\left(\frac{2\pi t}{T}\right) & i\sin\left(\frac{2\pi t}{T}\right) \\ i\sin\left(\frac{2\pi t}{T}\right) & \cos\left(\frac{2\pi t}{T}\right) \end{pmatrix}$$

We see then that each step of $U(t)$ is a swap between connected sites with a $\frac{\pi}{2}$ phase.

The evolution of the drive over the whole system is shown in fig 4.1b. The combination of 4 swaps brings particles that start in the bulk of the chain back to their starting point with the phases adding up to unity. The particles on the edges only receive two swaps, still returning to the starting point (as the unitary loop was inherently imposed to be the identity at the end) but with a phase of π instead. These boundary 'π modes' are a signature of topological Floquet phases(I feel like I need a reference here).

If we remind ourselves of the action of the chiral operator on the Hamiltonian and unitary

$$CH(t)C^{-1} = -H(-t)$$

$$CU(t)C^{-1} = U(T-t)U^{\dagger}(T)$$

we can see that the halfway time point of the drive commutes with the chiral symmetry operator. This is due to the fact that we have constructed our drive as a loop, so $U(0) = U(T) = \mathbb{1}$.

$$CU(T/2)C^{-1} = U(T/2)U^{\dagger}(T) = U(T/2)$$

This means that the midpoint unitary is diagonal with respect to chirality, or more simply can be written as block diagonal in its action on the A and B lattice sites.

$$U(T/2) = \begin{pmatrix} U_A & 0 \\ 0 & U_B \end{pmatrix}$$

In this drive, we can see that after the first two steps, there has been a swap of A and B within a cell, followed by a swap of A and B between neighboring cells. This means that A sites have moved one unit cell to the right and B sites have moved one site to the left. Therefore, in our case $U_A = \hat{t}$ and $U_B = \hat{t}^{\dagger}$ where $\hat{t}$ is a translation left by a single cell. A unitary translation cannot be generated by a finite set of local unitary transformations meaning the eigenstates of the unitary will be delocalized. This fact will be considered more in my own work later.

Given this model, X. Liu et. al were able to define a set of real space topological invariants that showed a bulk-boundary correspondence. This construction was based on Kitaev

who proved that such an invariant would be robust to disorder [Kit06]. This compares to the existing k-space invariants defined by [Fru16] which are ill-defined in the presence of disorder.

CHAPTER 5

Disordered Chiral Floquet Evolution

5.1 Overview

In chapter 4 we introduced the Floquet loop formalism and a simple 1D chiral Floquet model. In this chapter we will consider adding disorder to that model. We will introduce the class of models as well as our numerical techniques. Our main investigative probe will be the localization length of eigenstates of the unitary time evolution operator, sampled at times during its evolution. We find numerical evidence to support the existence of topologically protected delocalization and show universality.

5.2 Anderson Localization

It was Anderson, in 1958, who first formulated the problem of disordered systems their property of localization [And58]. As it became more understood, Mott [MT61] and later Thouless [Tho70, ATA73] showed that any amount of disorder is enough to exponentially localize every eigenstate for a 1D single particle lattice system. Rigorous proofs of this statement have been shown multiple times [GMP77, KS80] and rely on principles that will be touched upon in section 5.6 which discusses transfer matrices. However, these results are for Hamiltonian-type operators whose solutions obey Schrodinger type differential equations.

5.3 Disordered Unitaries

To extend the concepts of Anderson localization to unitary evolutions, we fast forward significantly to recent developments in the study of discrete time quantum unitary random walks. The concept of a random walk with a quantum coin was introduced by Aharonov et. al. [AAK01]. As opposed to a standard 1D random walk, where the walker moves left or right each time step at some probability, the quantum walker has two internal coin states, one left moving and one right moving. The state of the walker is comprised of a probability amplitude on each site n with left and right moving components. A time step of the walk involves acting with a unitary operation (the coin operator $\hat{\mathcal{C}}$) on the onsite Hilbert space of the walker at each position, followed by the shift operator (denoted by $\hat{S}$) of the left (right) moving part of the coin space to the coin space of the walker in the left (right) neighboring position.

$$\hat{\mathcal{C}} = \bigoplus_n \hat{\mathcal{C}}_n,\ \hat{\mathcal{C}}_n \in U(2) \text{ and } \hat{S} = \sum_n |n+1, \rightarrow\rangle\langle n, \rightarrow| + |n-1, \leftarrow\rangle\langle n, \leftarrow|$$

where the $\rightarrow$, $\leftarrow$ correspond to the right and left moving subspaces and n is summed over the different sites of the 1D system.

The different $\hat{\mathcal{C}}_n$ need not be the same, even sometimes changing each time step. Disordered models chose random unitaries from $U(2)$ or some subset at for their coin operators. In numerical models [KLM07, YKE08] and for continuous probability distributions with respect to the Haar measure [ASW11], the disordered quantum random walk displays dynamical localization. Dynamical localization is an exponential decay in the tunneling probabilities between sites as a function of distance and is equivalent to static Anderson localization in the space of eigenstates of the unitary evolution operator.

The well studied field of quantum random walks inspires our research into disordered Floquet evolutions. While our unitary operators are more specific, we can expect to see localization if we disorder our system. However, the topological nature of our drives means the physics will not always localize. Topological phases have shown to protect extended edge modes coexistent with Anderson localization of the bulk in quantum random walks

[OK11]. Additionally, disordered versions of class AIII static insulators have been shown to support a topological phase until a transition at strong disorder [MHS14]. The study of the AIII Floquet model predicts stability of the topological invariant under disorder [LHR18] and some work has looked at protected modes at specific quasienergies [Gan15]. We wish to understand the effects of disorder throughout the evolution of such a system.

5.4 Disordered Class AIII Floquet Insulator

Like the chiral Floquet chain, we consider a 1D spinless single particle tight binding model with chiral symmetry only (class AIII). Our evolution will be built from a series of static Hamiltonians which are each evolved for some time period.

$$H(t) = \begin{cases} H_1 & 0 \leq t < T_1 \\ H_2 & T_1 \leq t < T_2 \\ \vdots & \vdots \end{cases}$$

The model has two sublattice sites (A and B) per unit cell which gives an on-site Hilbert space dimension of 2. In general, the Hamiltonians (and corresponding unitary evolutions) that mix A and B degrees of freedom within a single unit cell will be referred to as 'trivial' and ones that connect unit cells will be referred to as 'topological'. Hamiltonians that only act on a single sublattice site will be referred to as 'static'.

Building on the chiral chain model, we initially consider the Hamiltonians:

$$H_1 = \sum_i a_i^\dagger b_i + b_i^\dagger a_i$$

$$H_2 = \sum_i a_{i+1}^\dagger b_i + b_i^\dagger a_{i+1}$$

$$H_d = \sum_i w_i^a a_i^\dagger a_i + w_i^b b_i^\dagger b_i$$

where $a_i^\dagger, a_i$ and $b_i^\dagger, b_i$ are the creation and annihilation operators for A and B sites in unit cell i, and the w are random potentials taken from a uniform distribution. Exponentiating

the matrix elements, we see that

$$U_1(t) = \sum_i \cos(t) a_i^\dagger a_i + \cos(t) b_i^\dagger b_i + i \sin(t) a_i^\dagger b_i + i \sin(t) b_i^\dagger a_i$$

$$U_2(t) = \sum_i \cos(t) a_{i+1}^\dagger a_{i+1} + \cos(t) b_i^\dagger b_i + i \sin(t) a_{i+1}^\dagger b_i + i \sin(t) b_i^\dagger a_{i+1}$$

$$U_d(t) = \sum_i e^{itw_i^a} a_i^\dagger a_i + e^{itw_i^b} b_i^\dagger b_i$$

This shows that evolution by $\frac{\pi}{2}$ gives us a unitary that directly swaps the respective adjacent sites and evolving for π gives the identity. Therefore, our total period T will be 2π as we consider a hopping strength of 1 for simplicity, but without loss of generality. From these unitaries we can create the loop

$$U(T) = U_d^{-1}\Big(\frac{1}{2}T_d\Big) U_1\Big(\frac{\pi}{2}\Big) U_2(\pi) U_1\Big(\frac{\pi}{2}\Big) U_d\Big(\frac{1}{2}T_d\Big)$$

where we have denoted a separate period of application for the disordered unitaries. As $U_1(t)$ and $U_2(t)$ are both the identity when evolved for $T/2 = \pi$ the full evolution is a loop in a trivial way.

Only applying the disorder at the beginning and the end of the evolution might seem artificial, but if we consider disordering the Hamiltonian itself

$$H_1 \to U_d^\dagger H_1 U_d$$

$$U_1 = e^{itH_1} \to e^{itU_d^\dagger H_1 U_d} =$$

$$\mathbb{1} + itU_d^\dagger H_1 U_d - \frac{i}{2} t^2 (U_d^\dagger H_1 U_d)^2 \dots$$

we see that

$$(U_d^\dagger H U_d)^n = U_d^\dagger H U_d U_d^\dagger H U_d \cdots = U_d^\dagger H^n U_d$$

so conjugating our unitary by the disorder is equivalent to disordering the Hamiltonian. Additionally, because we evolve $U_2(t)$ back to the identity, it does not matter if we disorder H_1 and H_2 in different ways as placing the disorder between U_1 and U_2 is equivalent.

As we saw in chapter 4, the combination of two swaps halfway through the drive gives a translation operator for A sites as well as B sites in opposite directions. The non-local nature

of the translation operator means that the eigenstates of the unitary will be extended at this time point. We also saw that this property is tied to a topological invariant that is robust to disorder so long as chiral symmetry is preserved. However, we saw that infinitesimal disorder will localize trivial unitary evolutions in an Anderson way, so there will be a topological phase transition. Between these two there will be a crossover region. The nature of delocalization as the system approaches the transition is the focus of our numerical analysis.

5.5 Numerical Methods: Exact Diagonalization

5.5.1 Preliminary Information

Given the matrix form of the unitary evolution, a direct way to probe the localization-delocalization transition of the drive is to generate and diagonalize $U(t)$ for a realization of disorder and then consider the localization length of its eigenstates. This method, known as exact diagonalization (or ED for short), is the natural first look at the effect as any Hamiltonian can be readily and directly implemented.

We can probe any time point during the evolution of the drive by evaluating the unitary up to that point and since the generating Hamiltonian is piecewise static, the simple rule for multiplication of unitary time evolutions applies

$$U(t_1)U(t_2) = U(t_1 + t_2)$$

For any specific U it allows us to look at some time point of our drive, $U_2(\Delta t)U_1(\pi/2)$, perform an analysis of the matrix, and then use the same unitary to generate the unitary at an adjacent time step $U_2(\Delta t)U_2(\Delta t)U_1(\pi/2) = U_2(2\Delta t)U_1(\pi/2)$. This forms a discretization of our evolution. The main advantage is we only need to keep in memory the unitary at the current point of analysis to progress to the next point and we can use the existing form for $U_2(t)$ to progress iteratively.

The localization length of an eigenstate, ϕ_n, in a system of size L is found by determining

the center of mass of ϕ_n using a periodic position operator (if in periodic BC):

$$x_n^{\text{COM}} = \frac{L}{2\pi}\text{Im}[\ln(\langle\phi_n|\hat{r}_x|\phi_n\rangle)]$$

$$\hat{r}_x = e^{2\pi i\hat{x}/L}$$

or just via the expectation of the position operator (in an open system). Given this, the localization length is defined as

$$\xi_n = \langle\phi_n||\Delta\hat{x}_n||\phi_n\rangle$$

$$\Delta x_n = x - x_n^{\text{COM}}$$

where the coordinate transformation centers the system on the center of the wavefunction and then the localization length is the mean deviation of the probability distribution. It is important to note that for an evenly distributed (i.e. constant or plane wave $\psi_n \propto e^{ik_n x}$) wavefunction, the ξ_n is half the distance to the edge on each side of the center as each point is equally probable. Therefore $\xi = L/4$ is the maximum localization length we can observe for a finite 1D system of length L with periodic boundary conditions.

Finally, instead giving an index to each wavefunction, it is convenient to label them by their quasienergy ϵ. The chiral drive starts as the identity which has a quasienergy spectrum completely degenerate on $\epsilon = 0$, but disorder smears the spectrum across the unit circle of quasienergies allowing for states to be uniquely identified by quasienergy.

5.5.2 Adding Disorder

To investigate localization length of disordered eigenstates, it is first useful to talk about what happens to the eigenstates of the non-disordered system over the course of the drive. The trivial Hamiltonian, H_1, hops only within each unit cell and is block diagonal. Therefore the eigenstates of the unitary are just the solutions to the two level system in their respective unit cells and zero everywhere else, essentially completely localized for the whole of U_1. As we begin acting U_2 however, even the most infinitesimal translation operator part of the total unitary paired with the discrete translation invariance of the Hamiltonians involved give a

plane wave component to the eigenstates for every point during the evolution of $U_2(t)U_1(\pi/2)$ for $t > 0$. This is the topologically protected translation part of the unitary.

For reasonably large disordering potentials w the disordering unitary becomes equivalent to random phases. Therefore we can disregard the disorder period T_d and set $t = 0$ at the beginning of the non-disordered part of the unitary.

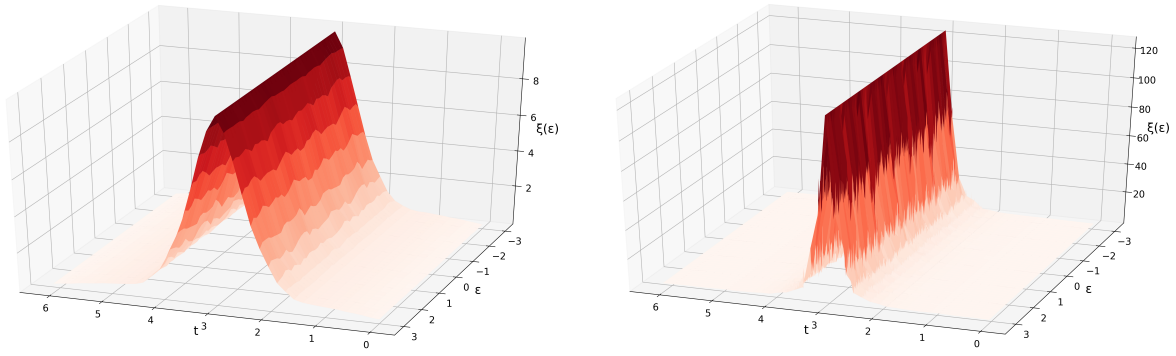

(a) 40 site chain with periodic boundary conditions over 40 time steps with 100 disorder realizations per step.

(b) 500 site chain with periodic boundary conditions over 40 time steps with 5 disorder realizations per step.

Figure 5.1: $\xi(\epsilon)$ plotted for $U(t)$ across the whole non-disorder part of the drive for a small system in 5.1a, where finite size effects round off the delocalization, and a larger system in 5.1b where the behavior is (at least visually) indicative of all larger systems of this unitary.

A plot of the disordered evolution in Fig 5.1 shows the localization length of all $\phi(\epsilon)$ over the course of the drive. What we see here is that every single eigenstate of the unitary evolution becomes delocalized, regardless of quasi-energy, at the midway point of the drive. Delocalization in the presence of disorder confirms that the topological properties of the clean drive are robust to disorder. It also means that for analysis, we will almost always average across eigenstates of U so as to take advantage of the drive's self averaging to require averaging together fewer disorder realizations. Chiral symmetry guarantees the drive to be symmetric around $T/2$ so we only need to do analysis of the first half of the evolution to investigate the properties of the drive.

Some limitations on the parameter space we can search with exact diagonalization is that solving larger system sizes L corresponds to finding the eigensystem of an $L \times L$ dimensional matrix which scales as, approximately $\mathcal{O}(L^{2.8})$ and therefore can be prohibitively long to calculate for large system sizes [PCZ98]. This means that you generally have smaller system sizes and more finite size effects. While the finite size scaling is possible for finding thermodynamic quantities, you must also choose a larger number of disorder realizations for smaller systems as an additional computational cost.

5.6 Numerical Methods: Transfer Matrix

5.6.1 Preliminary Information

Transfer matrix methods have been historically used to investigate Anderson localization. By considering the transport of current through a wire containing impurities, we solve for the electron wavefunction in a model problem of Anderson localization following the description put forth in ref [MD10].

We assume the electron is spinless and non-interacting for simplicity of the example. The impurities will be modeled as potential barriers that the electron must tunnel through, allowing us to approach the problem as a scattering problem. We will assume the impurity density n is sufficiently dilute ($n << k$) and their widths σ to be sufficiently narrow ($k\sigma << 1$) compared to the electron wavenumber k such that they can be modeled as delta function potentials and can be considered independently.

Assuming an incident plane wave, the simple quantum mechanical approach is to take general plane wave functions for the left (ψ_L) and right (ψ_R) side of the barrier and solve for the scattering matrix S from the boundary conditions.

$$\psi_L = \psi_L^{\text{in}} e^{+ikx} + \psi_L^{\text{out}} e^{-ikx}$$
$$\psi_R = \psi_R^{\text{in}} e^{+ikx} + \psi_R^{\text{out}} e^{-ikx}$$

$$\begin{pmatrix} \psi_L^{\text{out}} \\ \psi_R^{\text{out}} \end{pmatrix} = \begin{pmatrix} r & t' \\ t & r' \end{pmatrix} \begin{pmatrix} \psi_L^{\text{in}} \\ \psi_R^{\text{in}} \end{pmatrix}$$

The r, t (r', t') refer to the reflection and transmission coefficients for waves incident on the left (right) side of the barrier. Normalization of the wave function then becomes equivalent to probability conservation and we know our S-matrix is unitary. This allows us to relate r, r', t, t' for this simple case of a 2×2 S-matrix.

$$t' = t, \quad r' = \frac{r^* t}{t^*}$$

However, this configuration does not allow for the effects of one impurity to be combined with the effects of another in a simple way. Instead we want to split the wave function into right and left moving pieces (ψ^+ and ψ^- respectively) that span the whole length of the system and relate those pieces from one side of the obstacle to the other. This is equivalent to a reconfiguration of the original matrix equation.

$$\psi(x) = \psi^+ e^{+ikx} + \psi^- e^{-ikx}$$

$$\psi_L^{\text{in}} = \psi_L^+, \quad \psi_L^{\text{out}} = \psi_L^-, \quad \psi_R^{\text{in}} = \psi_R^-, \quad \psi_R^{\text{out}} = \psi_R^+$$

$$\begin{pmatrix} \psi_R^+ \\ \psi_R^- \end{pmatrix} = \begin{pmatrix} 1/t^* & -r^*/t^* \\ -r/t & 1/t \end{pmatrix} \begin{pmatrix} \psi_L^+ \\ \psi_L^- \end{pmatrix}$$

This matrix is the transfer matrix or T-matrix and allows us to combine the effect of obstructions in series. The wavefunction ψ_1 after the first obstacle is related to the initial wavefunction ψ_o by T_1

$$\psi_1 = T_1 \psi_o$$

and the wavefunction ψ_2 after the second obstacle is related to ψ_1 by T_2

$$\psi_2 = T_2 \psi_1 = T_2 T_1 \psi_o$$

We see a chaining effect occurring, and therefore, at the end of our system, we can relate the final transmitted wavefunction to our input wave after N impurities like so

$$\psi_N = T_N T_{N-1} \dots T_2 T_1 \psi_o = \mathbf{T}(N) \psi_o$$

and the transmission probability with the modulo square

$$|\psi_N|^2 = \psi_o^\dagger \mathbf{T}^\dagger \mathbf{T} \psi_o$$

where the matrix $\mathbf{M}(N) = \mathbf{T}^\dagger \mathbf{T}$ therefore encodes the entire system.

This is a Hermitian matrix and we can define the Lyapunov exponent

$$2\gamma = \lim_{N\to\infty} \frac{\langle \ln \mathbf{M}(N) \rangle}{N}$$

where the expectation value encodes a statement of ergodicity and self averaging as proven by Furstenberg [FK60, Fur63]. This quantity was introduced by Carmona in the efforts of giving a rigorous mathematical foundation to Anderson localization, and encodes the exponential decay of wavefunctions in a disordered system [Car82]

$$\gamma(E) = \lim_{x\to\infty} \frac{\ln |\psi(x,E)|}{x}$$

We acknowledge here that we picked a certain momentum k in the construction of transfer matrices which will correspond to a certain energy E. The Lyapunov exponents are real and positive [GMP77] which implies an exponential tail to our wavefunction

$$|\psi(x,E)|^2 \propto \exp(-2\gamma(E)x) = \exp(-x/\xi)$$

This means that by using the T-matrix method to calculate the Lyapunov exponent for a certain energy (or in our case quasienergy) we can calculate the localization length of the corresponding wavefunction at that energy. As our system is uniformly smeared onto all possible quasienergies, the existence of a state at any chosen quasienergy will be guaranteed.

5.6.2 Implementation

To see how our problem maps onto the T-matrix problem, we remind ourselves that during the action of H_2, our A sites are being swapped to the unit cell to the left and our B sites are similarly swapped to the right. This means that our A and B sites can be identified as left and right moving parts of the Hilbert space in each unit cell. This is exactly true

at the halfway point of the drive. Therefore, we can use the T-matrix formalism with the amplitude on A sites being ψ^+ and the amplitude on B sites being ψ^- and use the Lyapunov exponent to find the localization length of our wavefunctions.

Firstly let us re-state the matrix form of our unitary operators so as to calculate the analytical form of our T-matrix. Working in the position basis for an eigenstate of the unitary

$$\vec{\psi} = \left(\psi_1^A, \psi_1^B, \psi_2^A, \psi_2^B, \dots \psi_i^A, \psi_i^B, \dots \psi_L^A, \psi_L^B\right)$$

we can write down simple forms of each unitary. U_d is diagonal and $U_{1,2}$ are block diagonal matrices evocative of a rotation except for at the boundary where U_2 connects across the boundary only in a periodic system.

$$U_d = \begin{pmatrix} e^{i\phi_A(1)} & 0 & 0 & 0 \\ 0 & e^{i\phi_B(1)} & 0 & 0 \\ 0 & 0 & e^{i\phi_A(2)} & 0 \\ 0 & 0 & 0 & \ddots \end{pmatrix} \begin{matrix} \psi_1^A \\ \psi_1^B \\ \psi_2^A \\ \vdots \end{matrix}$$

$$U_1^i(t) = \begin{pmatrix} \cos(t) & i\sin(t) \\ i\sin(t) & \cos(t) \end{pmatrix} \begin{matrix} \psi_i^A \\ \psi_i^B \end{matrix} \qquad U_2^i(t) = \begin{pmatrix} \cos(t) & i\sin(t) \\ i\sin(t) & \cos(t) \end{pmatrix} \begin{matrix} \psi_i^B \\ \psi_{i+1}^A \end{matrix}$$

Combining these, we can write the total unitary $U_2(t)U_1(\pi/2)U_d$ as

$$U(t) = \begin{pmatrix} \ddots & 0 & 0 & 0 & 0 & 0 \\ 0 & 0 & e^{i\phi_B(2)}\sin(t) & 0 & 0 & 0 \\ 0 & 0 & ie^{i\phi_B(2)}\cos(t) & 0 & 0 & 0 \\ 0 & ie^{i\phi_A(2)}\cos(t) & 0 & 0 & e^{i\phi_B(3)}\sin(t) & 0 \\ 0 & e^{i\phi_A(2)}\sin(t) & 0 & 0 & ie^{i\phi_B(3)}\cos(t) & 0 \\ 0 & 0 & 0 & ie^{i\phi_A(3)}\cos(t) & 0 & 0 \\ 0 & 0 & 0 & e^{i\phi_A(3)}\sin(t) & 0 & 0 \\ 0 & 0 & 0 & 0 & 0 & \ddots \end{pmatrix}$$

By taking the middle pair of rows, we can write down a simple recurrence relation between unit cells using the eigenvalue equation. We leave the quasienergy as a free parameter.

$$U(t)\vec{\psi} = e^{-i\epsilon}\vec{\psi}$$

$$\Downarrow$$

$$ie^{i\phi_A(i)}\cos(t)\psi_i^A + e^{i\phi_B(i+1)}\sin(t)\psi_{i+1}^B = e^{-i\epsilon}\psi_i^B$$
$$e^{i\phi_A(i)}\sin(t)\psi_i^A + ie^{i\phi_B(i+1)}\cos(t)\psi_{i+1}^B = e^{-i\epsilon}\psi_{i+1}^A$$

We separate the equations by the unit cell they apply to.

$$\underbrace{\begin{pmatrix} ie^{i\phi_A(i)}\cos(t) & -e^{-i\epsilon} \\ e^{i\phi_A(i)}\sin(t) & 0 \end{pmatrix}}_{M_i}\begin{pmatrix} \psi_{A,i} \\ \psi_{B,i} \end{pmatrix} = \underbrace{\begin{pmatrix} 0 & -e^{i\phi_B(i+1)}\sin(t) \\ e^{-i\epsilon} & -ie^{i\phi_B(i+1)}\cos(t) \end{pmatrix}}_{N_{i+1}}\begin{pmatrix} \psi_{A,i+1} \\ \psi_{B,i+1} \end{pmatrix}$$

which finally allows us to write down the form of the transfer matrix

$$\begin{aligned}
\begin{pmatrix} \psi_{A,i+1} \\ \psi_{B,i+1} \end{pmatrix} &= N_{i+1}^{-1}M_i\begin{pmatrix} \psi_{A,i} \\ \psi_{B,i} \end{pmatrix} \\
&= \begin{pmatrix} -ie^{i\epsilon}\cot(t) & e^{i\epsilon} \\ -e^{-i\phi_B(i+1)}\csc(t) & 0 \end{pmatrix}\begin{pmatrix} ie^{i\phi_A(i)}\cos(t) & -e^{-i\epsilon} \\ e^{i\phi_A(i)}\sin(t) & 0 \end{pmatrix}\begin{pmatrix} \psi_{A,i} \\ \psi_{B,i} \end{pmatrix} \\
&= \begin{pmatrix} e^{i(\epsilon+\phi_A(i))}\csc(t) & i\cot(t) \\ -ie^{i(\phi_A(i)-\phi_B(i+1))}\cot(t) & e^{-i(\epsilon+\phi_B(i+1))}\csc(t) \end{pmatrix}\begin{pmatrix} \psi_{A,i} \\ \psi_{B,i} \end{pmatrix}
\end{aligned}$$

$$\begin{aligned}
\therefore T_i &= \begin{pmatrix} e^{i(\epsilon+\phi_A(i))}\csc(t) & i\cot(t) \\ -ie^{i(\phi_A(i)-\phi_B(i+1))}\cot(t) & e^{-i(\epsilon+\phi_B(i+1))}\csc(t) \end{pmatrix} \\
&= \begin{pmatrix} e^{i(\epsilon+\phi_A(i))}\sec(\tau) & i\tan(\tau) \\ -ie^{i(\phi_A(i)-\phi_B(i+1))}\tan(\tau) & e^{-i(\epsilon+\phi_B(i+1))}\sec(\tau) \end{pmatrix}
\end{aligned}$$

where we change variables to $\tau = \pi/2 - t$, as it is zero at the transition, for convenience of calculation as we will be investigating the physics close to the point $t = T/2$. Note that the disorder from one transfer matrix is completely decoupled from the disorder for the next.

This means we can generate matrices iteratively without storing the disorder strengths in memory.

Once we have the form of the T-matrix, we can follow the existing formalism

$$\mathbf{T}(L) = T_L T_{L-1} \dots T_2 T_1$$

$$\mathbf{M} = \mathbf{T}^\dagger \mathbf{T}$$

to be able to probe the long length scale physics near the delocalization transition. The localization length is calculated from the Lyapunov exponent as derived earlier. In practice we use the largest eigenvalue $\lambda_{\max}$ of $\mathbf{M}$ or the magnitude of a right or left incident wave to calculate the expectation value of our scattering matrix $\mathbf{M}$. The extra factor of 2 to compare with exact diagonalization where the A and B sites are spatially separated.

$$\xi = \frac{4N}{\ln(\lambda_{\max})}$$

Note that this calculates the localization length for states at a specific quasienergy. However, due to our disorder spreading states out across the whole quasienergy spectrum, we can safely assume there will be an eigenstate of our unitary at any quasienergy we choose. In practice, we choose a random quasienergy and find our results to be completely independent of that choice which agrees with exact diagonalization where we see the same localization length for each eigenstate.

For our calculations, we generate and multiply N transfer matrices to simulate the transfer across a system of N pairs of A and B sites. As each generation of T is microscopic instance of disorder, we get the self averaging as seen in exact diagonalization and our Anderson localization example. From exact diagonalization, we know that the system size must be larger than the localization length for accurate results. However, as our eigenvalue is exponentially decreasing in N/ξ away from the transition, the magnitude of the elements of the matrix becomes too large for the datatype for localization lengths much below the effective system length. We therefore re-scale the T-matrix at each step given a best guess of the localization length $\xi_o(\tau)$ from our exact diagonalization data.

$$T_i(\tau) \to r(\tau) T_i(\tau)$$

$$r = \exp(2/\xi_o)$$

$$\xi = \frac{4N}{\ln(\lambda') + 4N/\xi_o}$$

This allows us to probe a larger set of scales while maintaining accuracy. Our guess needs to be fairly close, but the leniency is greater the larger the localization length which allows us to easily probe close to the transition, the region where the exact diagonalization estimate is least accurate.

The main advantage of the transfer matrix method is that the finite size limitations we face are proportional the number of T-matrices we chain together, N. This means that our algorithmic scaling is very close to linear in our effective system size, allowing us to probe much longer lengths than exact diagonalization.

The drawback for the method is that we had to calculate the transfer matrix analytically, making it a difficult tool to investigate a broad range of models. Therefore, we will use transfer matrices as an independent method to check the accuracy of the results to very long localization lengths.

5.7 Delocalization Transition Power Law

We now consider the power law behavior of the topologically protected delocalization as well as finite size effects. We use a standard phase transition nomenclature and label our tuning parameter and power law in terms of deviation from the transition.

$$\xi_\infty = |t_c - t|^\nu \equiv \tau^\nu$$

where the critical time point is the halfway point of the drive. We use the term ξ_∞ to denote the thermodynamical localization length of the theoretical system. This differs from the actual numerical value we obtain by the effects of the finite size of our simulated system.

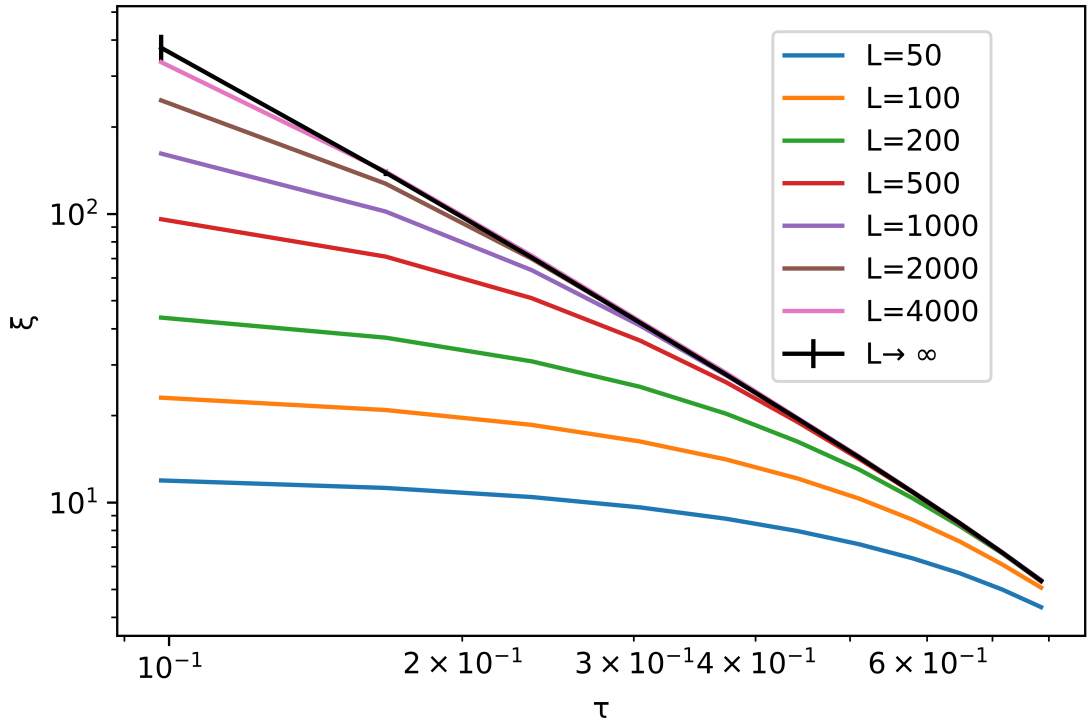

Figure 5.1: A log-log plot of average ξ of the exactly diagonalized onsite disordered drive. The x-axis, $\tau = T/2 - t$, measures the time away from the halfway point and ranges from $\frac{\pi}{32}$ to $\frac{\pi}{4}$. As the size increases, the trends converge towards a line which we fit below in figure 5.3. The error bars on the ξ_∞ fit are from the error of the fit of the finite size scaling and are too small to be seen except for the closest point to the transition.

5.7.1 Exact Diagonalization and Finite Size

A significant amount of the efforts of fitting data will be centered around the effects of finite size. As was briefly mentioned before, the limitation of finite size of the system puts a limit of $L/4$ on the maximum localization length of our exact diagonalization simulations. Therefore we will always see a rounding off as we approach the $t = T/2$ point where the localization length diverges.

We model the leading order effect of finite size in localization length coming from a single

scaling function

$$\xi(\tau, L) = \xi_\infty(\tau) - f(L, \tau)$$

where L is the size of the system we simulate and $f(L, \tau)$ is some unknown function that trends to zero as we approach the limit of $L \to \infty$.

A comparison of different fits for the scaling function that was used for calculating the line in figure 5.1 are shown for a single time point in figure 5.2. The exponential fit has the form

$$\xi(t, L) = \xi_\infty(t) - Ce^{-\alpha L}$$

while the power law test function used the form

$$\xi(t, L) = \xi_\infty(t) - CL^{-\alpha}$$

The comparison heavily favors the exponential fit and we extracted our values and errors for ξ_∞ from its fitting parameters. The exponent α and constant C are non-universal quantities and varied across the evolution, so we fit the data independently at each time point.

From the exponential fit, we can take the error from the covariance of the fit parameter. We used scipy's curve_fit utility for the fit. Given the error, we can perform a least squares fit of the ξ_∞ data, weighted to minimize the error function, and get an exponent for the power law scaling of 2.023 ± 0.015 (fig. 5.3). The error here only reflects statistical errors in the fitting, we see a clear downward bias close to the transition point that was accounted for as a systematic error in this number. As we move far from the transition point we see a deviation from the power law as well (fig. 5.4) giving us a finite range of meaningful data.

5.7.2 Transfer Matrix

The higher computational freedom for the transfer matrix model allows us a much greater ability to search the parameter space. Additionally, the lack of finite size effects as a hard limit of our simulation (compared to ED) avoids the need for a fit of finite size effects as we can easily simulate system sizes much greater than the localization length. A comparison and fit of the T-matrix data to ED is shown in figure 5.5. The fit line uses only data for

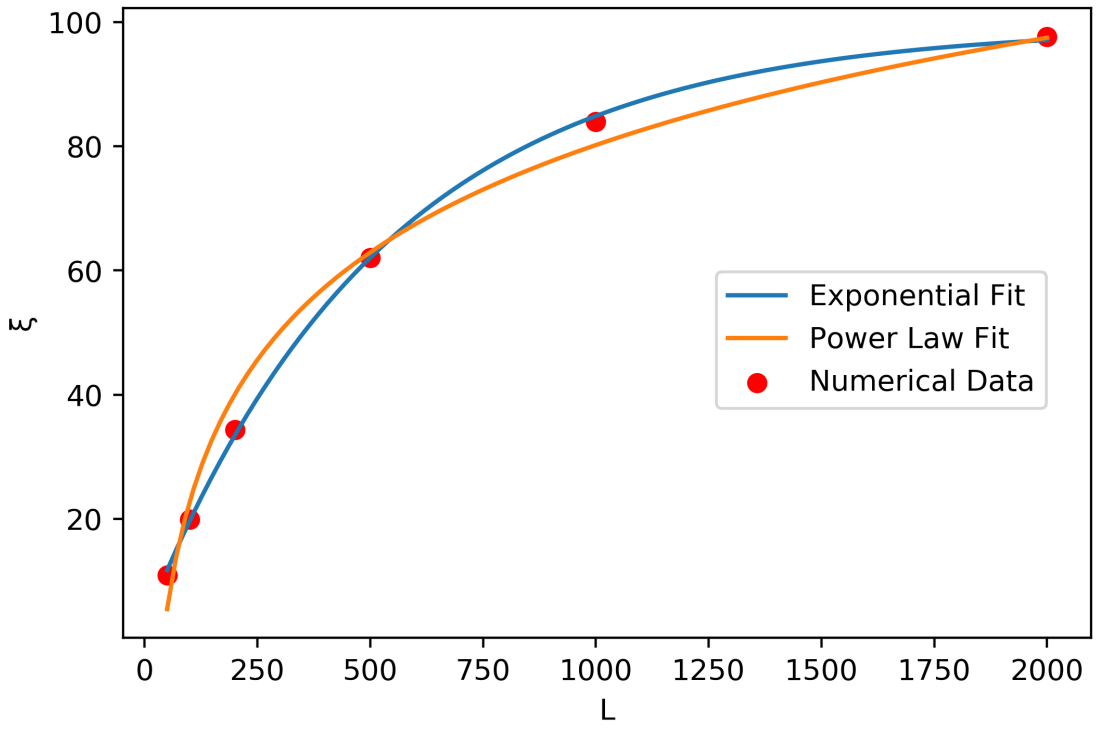

Figure 5.2: Length scaling for $\tau = \frac{\pi}{16}$ under exact diagonalization. The number of disorder realizations varies from 1000 down to 10 as the system size increases. The values of ξ_∞ obtained here are 96.2 for the exponential fit and 26500 for the power law fit, clearly favoring the hypothesis of an exponential scaling function.

$N = 500,000$ multiplications which corresponds to an effective system size of one million sites. The exponent from the fit gives 2.013 ± 0.004 which is consistent with the previous fit of the ED data and further supports the non-critical nature of data points far from the transition which deviate from the power law. As with the previous fit, the error in the exponent only includes least squares error in the fitting parameter. Due to the need for more leniency in the guessed parameters of $r(\tau)$, the T-matrix rescaling factor, we used a smaller value of N for the points further from the transition to compare to the ED data.

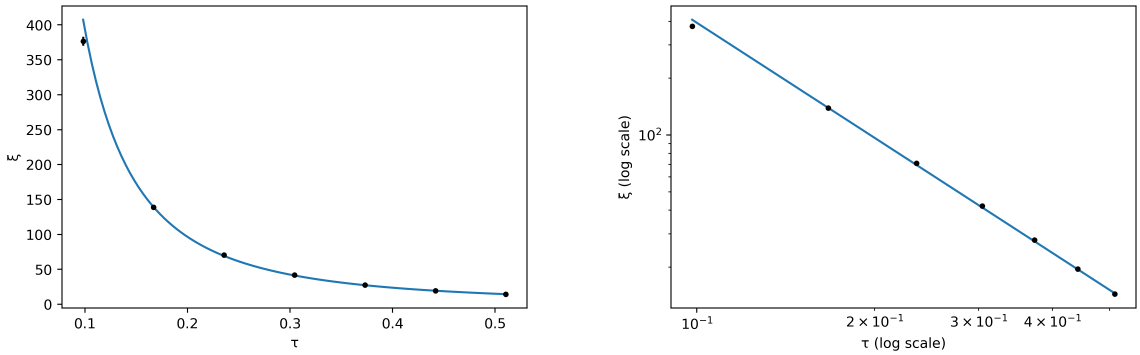

(a) (b)

Figure 5.3: Fitting ξ_∞ using exact diagonalization with errors. We fit the log data to a line and get a slope of 2.023 ± 0.015.

5.8 Universality

Until now we have discussed a single Hamiltonian with a single type of disorder. However our results apply to a whole class of models with equivalent topological properties within Class AIII called two band flattened models. A Class AIII Hamiltonian must have the block form

$$H_{\text{AIII}} = \begin{pmatrix} 0 & Q \\ Q^\dagger & 0 \end{pmatrix}$$

where Q is some matrix and we have chosen the chiral basis for our matrix where each term here is the block for the A and B sites with Q mixing the two. This is required to meet the symmetry condition that H_{AIII} anticommutes with the chiral symmetry operator

$$\{H_{\text{AIII}}, C\} = 0, \quad C = \begin{pmatrix} \mathbb{1} & 0 \\ 0 & -\mathbb{1} \end{pmatrix}$$

If we want flatness of the bands, it is equivalent to requiring the eigenvalues of H_{AIII} to be either ± 1. This can be done by choosing a unitary matrix $\mathcal{U}$ as our Q. In that case, $H^2 = \mathbb{1}$.

In the case of the model we considered initially, the matrix on the subspace, $\mathcal{U}$, is the identity, $\mathbb{1}$, for the trivial evolution (maps sublattice sites within the same unit cell) and a translation T (between unit cells) for the topological evolution. Within the class of flat

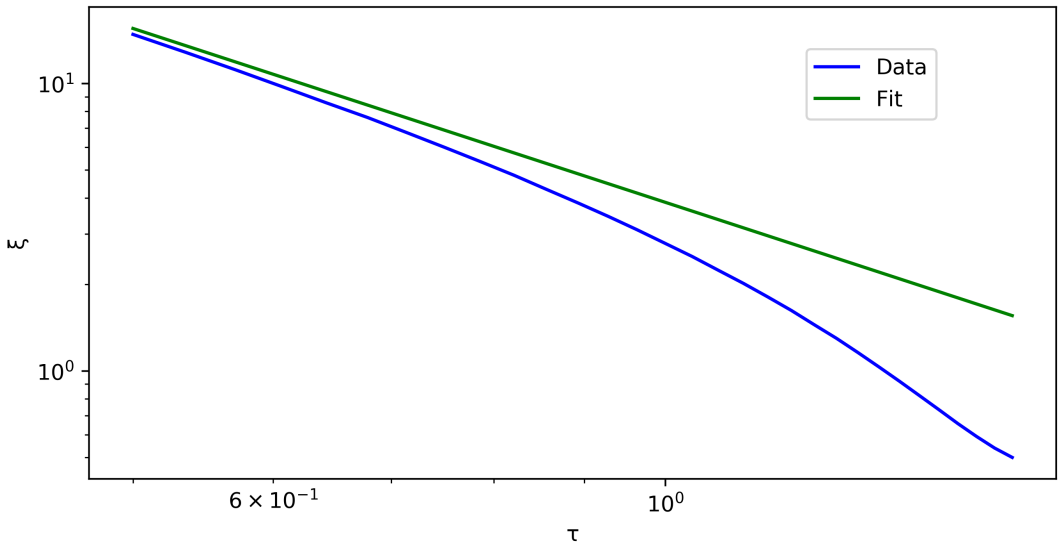

Figure 5.4: A plot of exact diagonalization data from the first half of the evolution of H_2. These points far from the transition point decay down to a localization length of 0.5 which is the only possible length for the evolution of H_1. When plotted versus the power law fit, we see a significant deviation due to this Hamiltonian specific dependence.

band Hamiltonians, this is always the case up to a unitary and differentiates topological and trivial evolutions

$$H_1 = \begin{pmatrix} 0 & \mathbb{1}\mathcal{U}_1 \\ \mathbb{1}\mathcal{U}_1^\dagger & 0 \end{pmatrix}, \quad H_2 = \begin{pmatrix} 0 & T^n\mathcal{U}_2 \\ T^n\mathcal{U}_2^\dagger & 0 \end{pmatrix}$$

Here T is the translation operator, so n represents the (non-zero) number of unit cells translated by the topological drive. This corresponds to the $\mathbb{Z}$ set of dynamical topological invariants for class AIII as seen on the periodic table 4.1. For our example, $n = 1$. There is the additional restriction on each $\mathcal{U}$ that it must be locally generated. This means that each $\mathcal{U}$ acts at any one site as a finite multiplication of nearest neighbor two site unitaries in an infinite system. As an example, the translation operator cannot be locally generated.

As we saw before when we constructed our unitary evolutions, the unitary time evolution of a flat band Hamiltonian has a convenient form

$$U = \exp(-itH) = \cos(t)\mathbb{1} - i\sin(t)H$$

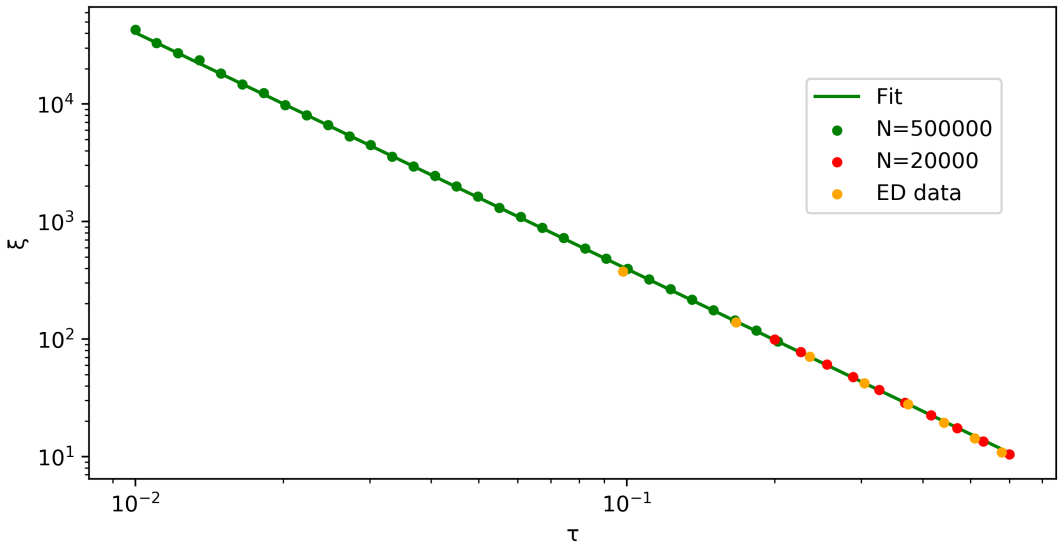

Figure 5.5: T-matrix data shown along with the data from exact diagonalization for comparison. The fit line is a power law fit for the $500,000$ T-matrix iteration data and has a slope of 2.013 ± 0.004 which is consistent with the previous fit. Lower iteration data (in red) is used to compare due for leniency of the T-matrix rescaling factor $r(\tau)$ as $N = 20,000$ is still multiple orders of magnitude above the localization length.

which makes the evolution at the point $t = T/2$ in the chiral basis for a general flat band AIII evolution

$$U(T/2) = U_2(\pi/2)U_1(\pi/2) = -H_2H_1 = -\begin{pmatrix} T\mathcal{U}_2^\dagger\mathcal{U}_1 & 0 \\ 0 & T\mathcal{U}_2\mathcal{U}_1^\dagger \end{pmatrix}$$

The total invariant of the full evolution is then the sum of the invariants of each part of the evolution and our full drive is topological with $n = 1$. Given this, we have picked an archetypical example for the topological phase. We have numerically tested and will show in the appendix 5.A.1 that longer translations in the topological phase reduce and have an equivalent T-matrix to the one we calculated for a single site translation. The very simple choice of locally generated unitary we used will be briefly discussed as well, but the delocalization is driven by the translation aspect of the drive and is blind to the structure of the local unitary for a model.

When considering disorder, we have already mentioned how our choice to factor the disorder out of the Hamiltonian for our calculation is valid. However, we see that we are also free to, within the universality class of flat band Hamiltonians, write the disordered evolution as an equivalent, albeit complicated, non-disordered AIII model. This comes from the fact that we have required our disorder to respect the chiral symmetry (that it does not connect A and B sites) and that the disorder is local (and therefore locally generated). We can see for the simple case of paired A and B disorder that

$$U_d = \begin{pmatrix} \mathcal{U}_d^\dagger & 0 \\ 0 & \mathcal{U}_d \end{pmatrix}, \quad U_1(\pi/2)U_d = \begin{pmatrix} 0 & \mathbb{1}\mathcal{U}_1\mathcal{U}_d \\ \mathbb{1}\mathcal{U}_1^\dagger\mathcal{U}_d^\dagger & 0 \end{pmatrix} = U_1', \quad \mathcal{U}_1' = \mathcal{U}_1\mathcal{U}_d$$

and that the evolution is equivalent to a different one within the same universality class. However it is also easy to use this same method to push a non-correlated form of disorder through to the center of the evolution where it cancels with its inverse on the second half of the loop

$$U_d(T/2) = U_2(\pi/2)U_1(\pi/2)U_d = -\begin{pmatrix} T\mathcal{U}_2^\dagger\mathcal{U}_1\mathcal{U}_{Ad} & 0 \\ 0 & T\mathcal{U}_2\mathcal{U}_1^\dagger\mathcal{U}_{Bd} \end{pmatrix}$$

$$\mathcal{U}_2^\dagger\mathcal{U}_1\mathcal{U}_{Ad} = \mathcal{U}_2^\dagger\mathcal{U}_{Ad}'\mathcal{U}_1' = \mathcal{U}_{Ad}''\mathcal{U}_2'^\dagger\mathcal{U}_1'$$

where pushing the disorder through a matrix switches the action of the disorder from A to B as one could expect

$$U_1' = U_{Ad}'^\dagger U_1 U_{Ad}, \quad U_1'^\dagger = U_{Bd}'^\dagger U_1^\dagger U_{Bd} \;\Rightarrow\; U_{Ad}' = U_{Bd}, \quad U_{Bd}' = U_{Ad}$$

In these ways, we are confident that our numerics encapsulates the topological properties of the symmetry group as opposed to a special case. Tests and checks of this more general formulation of disorder will also be considered in the appendix 5.A.2.

If we take the form of the unitary evolution at a point τ from the transition point, as we do in our calculations, we can see the τ dependence. By taking the exponentiated form of $U_2(t)$ in terms of sin and cos, we can write $U(\tau)$ in the chiral basis as

$$-\begin{pmatrix} T\mathcal{U}_2^\dagger\mathcal{U}_1\mathcal{U}_{Ad}\cos(\tau) & \mathbb{1}\mathcal{U}_1\mathcal{U}_{Bd}\sin(\tau) \\ \mathbb{1}\mathcal{U}_1^\dagger\mathcal{U}_{Ad}\sin(\tau) & T\mathcal{U}_2\mathcal{U}_1^\dagger\mathcal{U}_{Bd}\cos(\tau) \end{pmatrix}$$

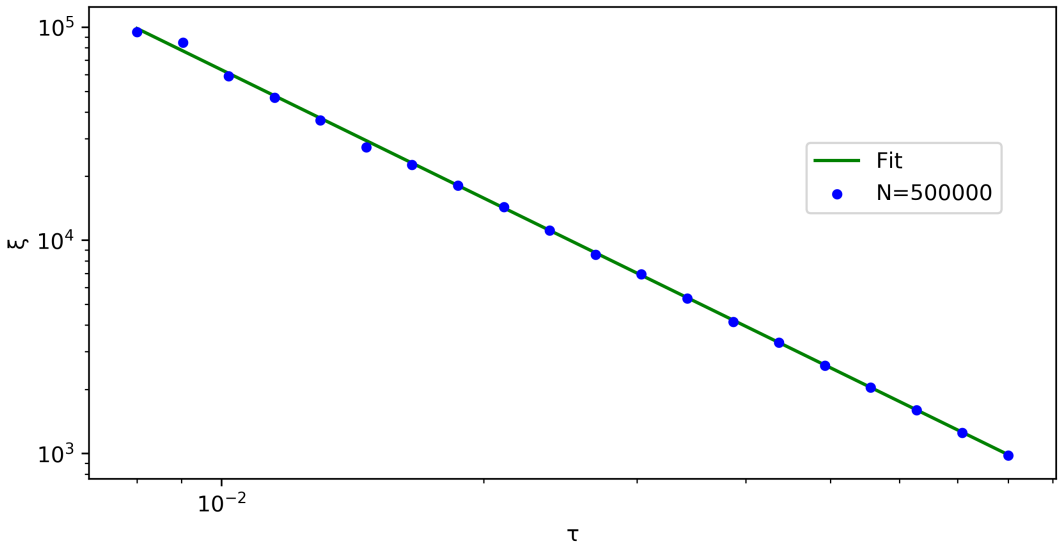

Figure 5.1: T-matrix data for N=5000 for the effective model of our system expanded in small τ. The fit line has a slope of 2.00 ± 0.01 which is the universal exponent that matches our numerics.

where the $\mathbb{1}$ only emphasizes that the total unitary acts trivially in that sector. Note that the positions of cos and sin have switched from the transformation from t to τ. We can write this in a simpler form in terms of our original Hamiltonians by representing the presence of disorder more generally as some general transformation over the whole non disordered part of the unitary $U(T) = U_d^{-1} U'(T) U_d$

$$U(\tau) = -\cos(\tau) H_2 H_1 U_d - i \sin(\tau) H_1 U_d$$

Here we see that the first term is topological and acts on the diagonal blocks of our chiral basis and the second is the off diagonal blocks and is trivial, as seen above. In that way, we can define $\mathcal{T}$ and $\mathcal{D}$ which correspond to the topological, translation part of the unitary and the trivial, disordered part, respectively. We can to this because a unitary that is the translation operator cannot be localized by a similarity transformation by a disorder unitary.

By then expanding in small τ we see the behavior near the transition as investigated by

our numerics

$$U(\tau) = -\mathcal{T} - i\tau\mathcal{D}$$

Here we see that, for small τ, it acts to leading order as a scaling of the disordered part of the unitary. Calculating the T-matrix for this toy model numerically (fig. 5.1) as well as analytic calculations (appendix 5.B.2) suggest that the localization length has a behavior which is proportional

$$\frac{1}{\xi} \propto \tau^2$$

for the principal model studied here [RH19] which gives a critical exponent of 2 and that more generally for flat band models, the localization length still retains a critical exponent of 2 [Bro].

5.A Generalizing Transfer Matrices

5.A.1 Different Hamiltonia

We wish to show that unitaries that function similarly to the onsite or intersite swap used in our numerics have an equivalently identical transfer matrix representation. Our next most simple example drive will be one that, instead of mixing A and B in cell for the trivial step, will mix the A and B sites of pairs of unit cells. The Hamiltonian for this step is

$$H_1 = \sum_i^{N/2} a_{2i+1}^\dagger b_{2i} + b_{2i+1}^\dagger a_{2i} + a_{2i}^\dagger b_{2i+1} + b_{2i}^\dagger a_{2i+1}$$

where i now indexes the larger unit cell. The equivalent exponentiation would look like

$$U_1^i(\pi/2) = \begin{pmatrix} 0 & 0 & 0 & -i \\ 0 & 0 & -i & 0 \\ 0 & -i & 0 & 0 \\ -i & 0 & 0 & 0 \end{pmatrix}$$

block diagonal for each pair of unit cells.

Using this extends our effective unit cell so when we write our system of equations for the transfer matrix, we get a system of 4 equations

$$\begin{aligned} ie^{i\phi_B(i)}\psi_{B,i}\cos(t) + e^{i\phi_C(i)}\psi_{C,i}\sin(t) &= e^{-i\epsilon}\psi_{C,i} \\ ie^{i\phi_A(i)}\psi_{A,i}\cos(t) + e^{i\phi_D(i+1)}\psi_{D,i+1}\sin(t) &= e^{-i\epsilon}\psi_{D,i} \\ e^{i\phi_A(i)}\psi_{A,i}\sin(t) + ie^{i\phi_D(i+1)}\psi_{D,i+1}\cos(t) &= e^{-i\epsilon}\psi_{A,i+1} \\ e^{i\phi_B(i+1)}\psi_{B,i+1}\sin(t) + ie^{i\phi_C(i+1)}\psi_{C,i+1}\cos(t) &= e^{-i\epsilon}\psi_{B,i+1} \end{aligned}$$

where C and D are the sublattice sites for the adjoining cell whereas i indexes the sites as in the Hamiltonian above. The transfer matrix links adjacent two-unit-cell blocks and we see this in the equations above. Only A and D have couplings across the unit cells where as

B and C are an independent internal block. The equations reduce and we are left with the same equation we had before to calculate the transfer matrix except with a larger effective unit cell

$$\begin{pmatrix} ie^{i\phi_A(i)}\cos(t) & -e^{-i\epsilon} \\ e^{i\phi_A(i)}\sin(t) & 0 \end{pmatrix} \begin{pmatrix} \psi_{A,i} \\ \psi_{D,i} \end{pmatrix} = \begin{pmatrix} 0 & -e^{i\phi_D(i+1)}\sin(t) \\ e^{-i\epsilon} & -ie^{i\phi_D(i+1)}\cos(t) \end{pmatrix} \begin{pmatrix} \psi_{A,i+1} \\ \psi_{D,i+1} \end{pmatrix}$$

We can see that choosing the trivial part of the drive to change was not special. As we are picking out parts of the total unitary for the system of equations to calculate the transfer matrix, changing the topological part in the same way would have just caused a shift in the indices, but no change to the equations. Indeed, when we explicitly implement this step in ED compared to the transfer matrix simplification we see the same physics. The main difference of either version of this evolution to the original calculation is that the effective unit cell size is reduced by a factor of 2, so we need a larger system size. The more the unitaries we use connects adjacent sites, the less useful ED becomes.

5.A.2 Different Disorder

This construction and calculation can be mirrored for an arbitrary random unitary connecting adjacent A sites and adjacent B sites (but not mixing to respect the symmetry). This disorder would have the form

$$U_{\mathrm{dis}U(2)} = \begin{pmatrix} u_{11}^{AC1} & 0 & u_{12}^{AC1} & 0 & 0 & 0 & 0 & 0 \\ 0 & u_{11}^{BD1} & 0 & u_{12}^{BD1} & 0 & 0 & 0 & 0 \\ u_{21}^{AC1} & 0 & u_{22}^{AC1} & 0 & 0 & 0 & 0 & 0 \\ 0 & u_{21}^{BD1} & 0 & u_{22}^{BD1} & 0 & 0 & 0 & 0 \\ 0 & 0 & 0 & 0 & u_{11}^{AC2} & 0 & u_{12}^{AC2} & 0 \\ 0 & 0 & 0 & 0 & 0 & u_{11}^{BD2} & 0 & u_{12}^{BD2} \\ 0 & 0 & 0 & 0 & u_{21}^{AC2} & 0 & u_{22}^{AC2} & 0 \\ 0 & 0 & 0 & 0 & 0 & u_{21}^{BD2} & 0 & u_{22}^{BD2} \end{pmatrix}$$

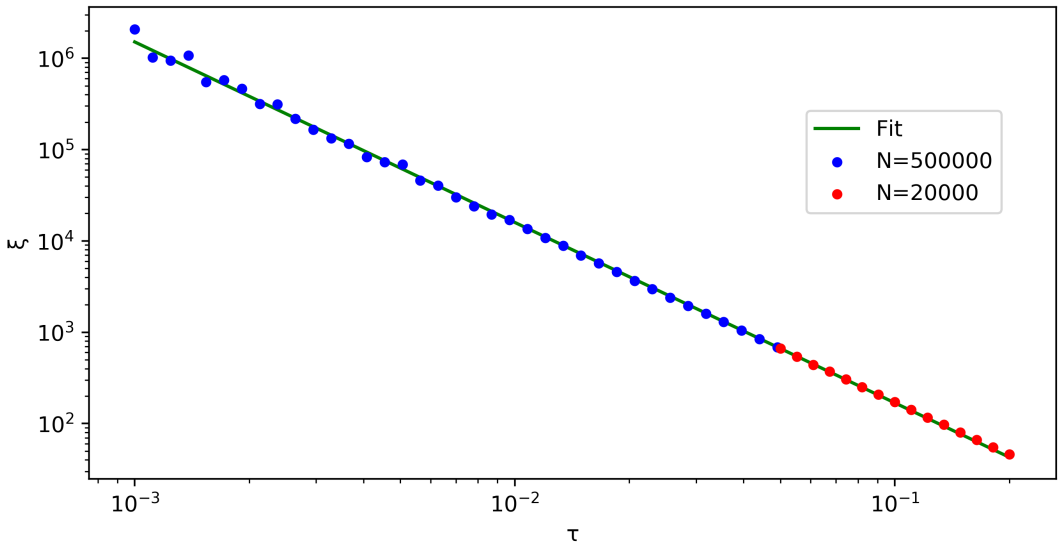

Figure 5.A.1: T-matrix data for the longer ranged unitary disorder. The fit line is a power law fit for just the data on 500000 T-matrix iterations and has a slope of 1.976 ± 0.008 which is close to the previous fit. Lower iteration data (in red) is used due for leniency of the T-matrix rescaling factor $r(\tau)$ and is consistent with the fit as well.

which acts as a U(2) matrix

$$\begin{pmatrix} u_{11} & u_{12} \\ u_{21} & u_{22} \end{pmatrix}$$

between sites A and C in each unit cell, and a different U(2) matrix between sites B and D of the doubled unit cell. This gives us the system of equations for the recurrence relation

$$\begin{aligned} &I\psi_{A,i}u_{11}^{AC}(i)\cos(t) + \psi_{B,i}u_{21}^{BD}(i)\sin(t) \\ &+ i\psi_{C,i}u_{12}^{AC}(i)\cos(t) + \psi_{D,i}u_{22}^{BD}(i)\sin(t) = e^{-i\epsilon}\psi_{B,i} \end{aligned}$$

$$\begin{aligned} &\psi_{A,i}u_{11}^{AC}(i)\sin(t) + i\psi_{B,i}u_{21}^{BD}(i)\cos(t) \\ &+ \psi_{C,i}u_{12}^{AC}(i)\sin(t) + i\psi_{D,i}u_{22}^{BD}(i)\cos(t) = e^{-i\epsilon}\psi_{C,i} \end{aligned}$$

$$\begin{aligned} &i\psi_{A,i}u_{21}^{AC}(i)\cos(t) + \psi_{B,i+1}u_{11}^{BD}(i+1)\sin(t) \\ &+ i\psi_{C,i}u_{22}^{AC}(i)\cos(t) + \psi_{D,i+1}u_{12}^{BD}(i+1)\sin(t) = e^{-i\epsilon}\psi_{D,i} \end{aligned}$$

$$\begin{aligned} &\psi_{A,i}u_{21}^{AC}(i)\sin(t) + i\psi_{B,i+1}u_{11}^{BD}(i+1)\cos(t) \\ &+ \psi_{C,i}u_{22}^{AC}(i)\sin(t) + i\psi_{D,i+1}u_{12}^{BD}(i+1)\cos(t) = e^{-i\epsilon}\psi_{A,i+1} \end{aligned}$$

$$\begin{aligned} &i\psi_{A,i+1}u_{11}^{AC}(i+1)\cos(t) + \psi_{B,i+1}u_{21}^{BD}(i+1)\sin(t) \\ &+ i\psi_{C,i+1}u_{12}^{AC}(i+1)\cos(t) + \psi_{D,i+1}u_{22}^{BD}(i+1)\sin(t) = e^{-i\epsilon}\psi_{B,i+1} \end{aligned}$$

$$\begin{aligned} &\psi_{A,i+1}u_{11}^{AC}(i+1)\sin(t) + i\psi_{B,i+1}u_{21}^{BD}(i+1)\cos(t) \\ &+ \psi_{C,i+1}u_{12}^{AC}(i+1)\sin(t) + i\psi_{D,i+1}u_{22}^{BD}(i+1)\cos(t) = e^{-i\epsilon}\psi_{C,i+1} \end{aligned}$$

The first two and last two equations are contained completely within their respective unit cells. They allow us to solve for and eliminate $\psi_{B,i}, \psi_{C,i}, \psi_{B,i+1}, \psi_{C,i+1}$ in terms of the re-

maining A and D wave function components. This leaves us with the matrix equation

$$\begin{pmatrix} iu_{21}^{AC}(i)\cos(t) & 0 & iu_{22}^{AC}(i)\cos(t) & -e^{-i\epsilon} \\ u_{21}^{AC}(i)\sin(t) & 0 & u_{22}^{AC}\sin(t) & 0 \end{pmatrix} \begin{pmatrix} \psi_{A,i} \\ \psi_{B,i} \\ \psi_{C,i} \\ \psi_{D,i} \end{pmatrix}$$

$$= \begin{pmatrix} 0 & -u_{11}^{BD}(i+1)\sin(t) & 0 & -u_{12}^{BD}(i+1)\sin(t) \\ e^{-i\epsilon} & -iu_{11}^{BD}(i+1)\cos(t) & 0 & -iu_{12}^{BD}(i+1)\cos(t) \end{pmatrix} \begin{pmatrix} \psi_{A,i+1} \\ \psi_{B,i+1} \\ \psi_{C,i+1} \\ \psi_{D,i+1} \end{pmatrix}$$

using Mathematica to compute the explicit form of the B and C components, this matrix equation reduces to the form

$$\begin{pmatrix} \psi_{A,i+1} \\ \psi_{D,i+1} \end{pmatrix} = \begin{pmatrix} M_{AA} & M_{AD} \\ M_{DA} & M_{DD} \end{pmatrix} \begin{pmatrix} \psi_{A,i} \\ \psi_{D,i} \end{pmatrix}$$

where $M_{AA}, M_{AD}, M_{DA}, M_{DD}$ are coefficient fractions that depend on the time, the components of the disordering unitary, and the quasienergy and are too large to quote here. This is our analytic form of the transfer matrix. By randomly generating the random unitary components and choosing an eigenquasienergy as in the original T-matrix formulation, we can numerically calculate the form and perform a similar analysis as before (see fig. 5.A.1). While a little more computationally heavy, the calculation is similar and shows the expected physics. Note that we use the whole disorder unitary for each cell, so we must store one disorder unitary between iterations.

5.B Analytic T-matrix Calculation

5.B.1 Methods and First Order Calculation

This section is based on unpublished notes and discussions [RH19].

From our simplified model of the divergence, we can write the recurrence relation equation

$$ie^{i\phi_A(i)}\tau\psi_i^A + \psi_{i+1}^B = e^{-i\epsilon}\psi_i^B$$
$$\psi_i^A + ie^{i\phi_B(i+1)}\tau\psi_{i+1}^B = e^{-i\epsilon}\psi_{i+1}^A$$

which can be reduced to the transfer matrix

$$\begin{aligned} T_i &= \begin{pmatrix} e^{i\epsilon} & ie^{i\phi_B(i+1)}\tau \\ -ie^{i\phi_A(i)}\tau & e^{-i\epsilon} \end{pmatrix} \\ &= \begin{pmatrix} e^{i\epsilon} & 0 \\ 0 & e^{-i\epsilon} \end{pmatrix} + \tau \begin{pmatrix} 0 & ie^{i\phi_B(i+1)} \\ -ie^{i\phi_A(i)} & 0 \end{pmatrix} \end{aligned}$$

For more detail on these steps, please refer to section 5.6.2 where we initially derived the transfer matrix for our system.

If we multiply N transfer matrices together and only keep to first order in τ, we see the following coefficient matrices

$$\mathbf{T}(N) = \begin{pmatrix} e^{iN\epsilon} & 0 \\ 0 & e^{-iN\epsilon} \end{pmatrix} + \tau \begin{pmatrix} 0 & i\sum_{i=0}^{N} e^{i(\phi_B(i+1)+(N-1)\epsilon)} \\ -i\sum_{i=0}^{N} e^{i(\phi_A(i)-(N-1)\epsilon)} & 0 \end{pmatrix}$$

We can, however, redefine each ϕ_A and ϕ_B to absorb the offset due to the factors of ϵ as they are random phases. This means the coefficient on τ is a sum of random phases. However, this does not mean the coefficient for the Lyapunov exponent is zero. If we take find $\mathbf{M}$ we confirm that to first order in τ our dependence on ϵ disappears

$$\mathbf{M} = \mathbf{T}^\dagger\mathbf{T} \; = \begin{pmatrix} 1 & i^N\tau\sum_{i=0}^{N}\left[e^{i\phi'_B(i+1)} + e^{-i\phi'_A(i)}\right] \\ (-i)^N\tau\sum_{i=0}^{N}\left[e^{i\phi'_A(i)} + e^{-i\phi'_B(i+1)}\right] & 1 \end{pmatrix}$$

The function for an incident plane wave gives us the localization length

$$\begin{aligned} \xi &= 4N\ln\left(\left|\left|\begin{pmatrix} 1 \\ (-i)^N\tau\sum_{i=0}^{N}\left[e^{i\phi'_A(i)} + e^{-i\phi'_B(i+1)}\right] \end{pmatrix}\right|\right)^{-1} \\ &= 4N\ln\left(\sqrt{1+\tau^2\sum_{i=1}^{N}\left[e^{i\phi'_A(i)} + e^{-i\phi'_B(i+1)}\right]\sum_{j=1}^{N}\left[e^{-i\phi'_A(j)} + e^{i\phi'_B(j+1)}\right]}\right)^{-1} \end{aligned}$$

and we see we depend on the mean square value of the sum.

$$\left|\sum_{i=0}^{N} e^{i\phi(i)}\right|^2 = \sum_{i=0}^{N} e^{i\phi(i)} \sum_{j=1}^{N} e^{-i\phi(j)} = \sum_{i=0}^{N} 1 + \sum_{i\neq j} e^{i(\phi(i)-\phi(j))}$$
$$= N$$

On average, the mod square is just proportional to the number of elements. However we have broken our order of approximation in doing so. There are no terms in the Lyapunov exponent of order τ, regardless of if we take an initial state, the largest exponent, or the trace. Therefore we require a calculation to the next order in the initial taylor series.

5.B.2 Second Order Calculation

To compute the second order correction for the toy model (see fig. 5.1), we start by expanding the $\cos(\tau)$ term to the next order

$$U(\tau) = -\mathcal{T}(1-\tau^2/2) - i\tau\mathcal{D}$$

which gives the recurrance relation

$$ie^{i\phi_A(i)}\tau\psi_i^A + (1-\tau^2/2)\psi_{i+1}^B = e^{-i\epsilon}\psi_i^B$$
$$(1-\tau^2/2)\psi_i^A + ie^{i\phi_B(i+1)}\tau\psi_{i+1}^B = e^{-i\epsilon}\psi_{i+1}^A$$

which gives us a transfer matrix of

$$T_i = \begin{pmatrix} e^{i\epsilon}(1-\tau^2/2 + \frac{\tau^2 e^{i(\phi_A(i)+\phi_B(i+1))}}{1-\tau^2/2}) & \frac{ie^{i\phi_B(i+1)}\tau}{1-\tau^2/2} \\ \frac{-ie^{i\phi_A(i)}\tau}{1-\tau^2/2} & \frac{e^{-i\epsilon}}{(1-\tau^2/2)} \end{pmatrix}$$

Here we can pull out a factor of $(1-\tau^2/2)^{-1}$ to simplify things. This factor will scale predictably, and the remaining matrix will be denoted by T_i'. Using this form, we can consider the action of multiple transfer matrices to get a form of the T-matrix as a function of N number of multiplications. If we look at the form of localization length, we see that the prefactor of $(1-\tau^2)^{-N}$ pulls right out

$$\begin{aligned}\frac{1}{\xi} &= \frac{1}{2N}\ln\big(\mathbf{T}^\dagger\mathbf{T}\ \big) \\ &= \ln\big(1+\tau^2/4\big) + \ln\Big(\mathbf{M'}^{\frac{1}{2N}}\Big)\end{aligned}$$

The first term gives the expected factor of τ^{-2}, the scattering matrix in the second term is shown in [RH19] to scale linearly in N

$$\begin{aligned}\mathbf{M} &\approx 1+\tau^2\mathcal{O}(N) \\ \ln\Big(\mathbf{M'}^{\frac{1}{2N}}\Big) &= \ln\Big((1+\tau^2\mathcal{O}(N))^{\frac{1}{2N}}\Big) \\ \lim_{N\to\infty}(1+aN)^{\frac{1}{N}} &= 1\end{aligned}$$

so the second term does not contribute in the thermodynamic limit and only the expected scaling remains.

BIBLIOGRAPHY

[AA81] H Aoki and T Ando. "EFFECT OF LOCALIZATION ON THE HALL CONDUCTIVITY IN THE TWO-DIMENSIONAL SYSTEM IN STRONG MAGNETIC FIELDS." *Solid State Communications11*, **38**:1079–1082, 1981.

[AAK01] Dorit Aharonov, Andris Ambainis, Julia Kempe, and Umesh Vazirani. "Quantum Walks on Graphs." In *Proceedings of the Thirty-third Annual ACM Symposium on Theory of Computing*, STOC '01, pp. 50–59, New York, NY, USA, 2001. ACM. event-place: Hersonissos, Greece.

[AF15] Yoichi Ando and Liang Fu. "Topological Crystalline Insulators and Topological Superconductors: From Concepts to Materials." *Annual Review of Condensed Matter Physics*, **6**(1):361–381, March 2015. arXiv: 1501.00531.

[AMV18] N. P. Armitage, E. J. Mele, and Ashvin Vishwanath. "Weyl and Dirac semimetals in three-dimensional solids." *Reviews of Modern Physics*, **90**(1):015001, January 2018.

[And58] P. W. Anderson. "Absence of Diffusion in Certain Random Lattices." *Physical Review*, **109**(5):1492–1505, March 1958.

[ASW11] Andre Ahlbrecht, Volkher B. Scholz, and Albert H. Werner. "Disordered quantum walks in one lattice dimension." *Journal of Mathematical Physics*, **52**(10):102201, October 2011.

[ASZ95] J. E. Avron, R. Seiler, and P. G. Zograf. "Viscosity of Quantum Hall Fluids." *Physical Review Letters*, **75**(4):697–700, July 1995.

[ATA73] R Abou-Chacra, D J Thouless, and P W Anderson. "A selfconsistent theory of localization." *Journal of Physics C: Solid State Physics*, **6**(10):1734–1752, May 1973.

[AZ97] Alexander Altland and Martin R. Zirnbauer. "Nonstandard symmetry classes in mesoscopic normal-superconducting hybrid structures." *Physical Review B*, **55**(2):1142–1161, January 1997.

[Ber84] Berry Michael Victor. "Quantal phase factors accompanying adiabatic changes." *Proceedings of the Royal Society of London. A. Mathematical and Physical Sciences*, **392**(1802):45–57, March 1984.

[BGR12] Barry Bradlyn, Moshe Goldstein, and N. Read. "Kubo formulas for viscosity: Hall viscosity, Ward identities, and the relation with conductivity." *Physical Review B*, **86**(24):245309, December 2012.

[Bis13] Rudro R. Biswas. "Semiclassical theory of viscosity in quantum Hall states." November 2013.

[Bot59] Raoul Bott. "The Stable Homotopy of the Classical Groups." *Annals of Mathematics*, **70**(2):313–337, 1959.

[Bro] A. Brown. "unpublished notes.".

[Car82] RenÃ© Carmona. "Exponential localization in one dimensional disordered systems." *Duke Mathematical Journal*, **49**(1):191–213, March 1982.

[CDS19] N. R. Cooper, J. Dalibard, and I. B. Spielman. "Topological bands for ultracold atoms." *Reviews of Modern Physics*, **91**(1):015005, March 2019.

[Che46] Shiing-shen Chern. "Characteristic Classes of Hermitian Manifolds." *Annals of Mathematics*, **47**(1):85–121, 1946.

[CTS16] Ching-Kai Chiu, Jeffrey C. Y. Teo, Andreas P. Schnyder, and Shinsei Ryu. "Classification of topological quantum matter with symmetries." *Reviews of Modern Physics*, **88**(3), August 2016. arXiv: 1505.03535.

[FK60] H. Furstenberg and H. Kesten. "Products of Random Matrices." *The Annals of Mathematical Statistics*, **31**(2):457–469, 1960.

[FKM07] Liang Fu, C. L. Kane, and E. J. Mele. "Topological Insulators in Three Dimensions." *Physical Review Letters*, **98**(10):106803, March 2007.

[Fru16] Michel Fruchart. "Complex classes of periodically driven topological lattice systems." *Physical Review B*, **93**(11):115429, March 2016.

[Fur63] Harry Furstenberg. "Noncommuting random products." *Transactions of the American Mathematical Society*, **108**(3):377–428, 1963.

[Gan15] Yuval Gannot. "Effects of Disorder on a 1-D Floquet Symmetry Protected Topological Phase." *arXiv:1512.04190 [cond-mat]*, December 2015. arXiv: 1512.04190.

[GMP77] I. Ya. Gol'dshtein, S. A. Molchanov, and L. A. Pastur. "A pure point spectrum of the stochastic one-dimensional schrÃ¶dinger operator." *Functional Analysis and Its Applications*, **11**(1):1–8, January 1977.

[GMP86] S. M. Girvin, A. H. MacDonald, and P. M. Platzman. "Magneto-roton theory of collective excitations in the fractional quantum Hall effect." *Physical Review B*, **33**(4):2481–2494, February 1986.

[GT18] Gian Michele Graf and Clément Tauber. "Bulk–Edge Correspondence for Two-Dimensional Floquet Topological Insulators." *Annales Henri Poincaré*, **19**(3):709–741, March 2018.

[Hal82] B. I. Halperin. "Quantized Hall conductance, current-carrying edge states, and the existence of extended states in a two-dimensional disordered potential." *Physical Review B*, **25**(4):2185–2190, February 1982.

[Hal88] F. D. M. Haldane. "Model for a Quantum Hall Effect without Landau Levels: Condensed-Matter Realization of the "Parity Anomaly"." *Physical Review Letters*, **61**(18):2015–2018, October 1988.

[HBJ18] Fenner Harper, David Bauer, T. S. Jackson, and Rahul Roy. "Finite-wave-vector

electromagnetic response in lattice quantum Hall systems." *Physical Review B*, **98**(24):245303, December 2018.

[HK10] M. Z. Hasan and C. L. Kane. "Colloquium : Topological insulators." *Reviews of Modern Physics*, **82**(4):3045–3067, November 2010.

[KDP80] K. v. Klitzing, G. Dorda, and M. Pepper. "New Method for High-Accuracy Determination of the Fine-Structure Constant Based on Quantized Hall Resistance." *Physical Review Letters*, **45**(6):494–497, August 1980.

[Kit03] A. Yu. Kitaev. "Fault-tolerant quantum computation by anyons." *Annals of Physics*, **303**(1):2–30, January 2003.

[Kit06] Alexei Kitaev. "Anyons in an exactly solved model and beyond." *Annals of Physics*, **321**(1):2–111, January 2006. arXiv: cond-mat/0506438.

[Kit09] Alexei Kitaev. "Periodic table for topological insulators and superconductors." *AIP Conference Proceedings*, **1134**(1):22–30, May 2009.

[Kli86] Klaus von Klitzing. "The quantized Hall effect." *Reviews of Modern Physics*, **58**(3):519–531, July 1986.

[KLM07] J. P. Keating, N. Linden, J. C. F. Matthews, and A. Winter. "Localization and its consequences for quantum walk algorithms and quantum communication." *Physical Review A*, **76**(1):012315, July 2007.

[KM05a] C. L. Kane and E. J. Mele. "Quantum Spin Hall Effect in Graphene." *Physical Review Letters*, **95**(22):226801, November 2005.

[KM05b] C. L. Kane and E. J. Mele. "$\{Z\}_\{2\}$ Topological Order and the Quantum Spin Hall Effect." *Physical Review Letters*, **95**(14):146802, September 2005.

[Koh85] Mahito Kohmoto. "Topological invariant and the quantization of the Hall conductance." *Annals of Physics*, **160**:343–354, April 1985.

[KS80] HervÃ© Kunz and Bernard Souillard. "Sur le spectre des opÃ©rateurs aux diffÃ©rences finies alÃ©atoires." *Communications in Mathematical Physics*, **78**(2):201–246, December 1980.

[KWB07] Markus König, Steffen Wiedmann, Christoph Brüne, Andreas Roth, Hartmut Buhmann, Laurens W. Molenkamp, Xiao-Liang Qi, and Shou-Cheng Zhang. "Quantum Spin Hall Insulator State in HgTe Quantum Wells." *Science*, **318**(5851):766–770, November 2007.

[Lau81] R. B. Laughlin. "Quantized Hall conductivity in two dimensions." *Physical Review B*, **23**(10):5632–5633, May 1981.

[LHR18] Xu Liu, Fenner Harper, and Rahul Roy. "Chiral flow in one-dimensional Floquet topological insulators." *Physical Review B*, **98**(16), October 2018.

[LW16] Rui Lin and Zhi Wang. "A brief review on Majorana bound states in topological superconductors." *Science China Physics, Mechanics & Astronomy*, **59**(7):677401, April 2016.

[MD10] Cord A. MÃ$\frac{1}{4}$ller and Dominique Delande. "Disorder and interference: localization phenomena." *arXiv:1005.0915 [cond-mat, physics:quant-ph]*, May 2010. arXiv: 1005.0915.

[MHS14] Ian Mondragon-Shem, Taylor L. Hughes, Juntao Song, and Emil Prodan. "Topological Criticality in the Chiral-Symmetric AIII Class at Strong Disorder." *Physical Review Letters*, **113**(4):046802, July 2014.

[MT61] N. F. Mott and W. D. Twose. "The theory of impurity conduction." *Advances in Physics*, **10**(38):107–163, April 1961.

[MV97] Nicola Marzari and David Vanderbilt. "Maximally localized generalized Wannier functions for composite energy bands." *Physical Review B*, **56**(20), November 1997.

[NN81] H. B. Nielsen and M. Ninomiya. "Absence of neutrinos on a lattice: (II). Intuitive topological proof." *Nuclear Physics B*, **193**(1):173–194, December 1981.

[OK11] Hideaki Obuse and Norio Kawakami. "Topological phases and delocalization of quantum walks in random environments." *Physical Review B*, **84**(19):195139, November 2011.

[OPA19] Tomoki Ozawa, Hannah M. Price, Alberto Amo, Nathan Goldman, Mohammad Hafezi, Ling Lu, Mikael C. Rechtsman, David Schuster, Jonathan Simon, Oded Zilberberg, and Iacopo Carusotto. "Topological photonics." *Reviews of Modern Physics*, **91**(1):015006, March 2019.

[PCZ98] Victor Y. Pan, Zhao Q. Chen, and Ailong Zheng. "The Complexity of the Algebraic Eigenproblem.", 1998.

[Pra81] R. E. Prange. "Quantized Hall resistance and the measurement of the fine-structure constant." *Physical Review B*, **23**(9):4802–4805, May 1981.

[PRS12] Siddharth A. Parameswaran, R Roy, and S. L Sondhi. "Fractional Chern insulators and the W_∞ algebra." *Phys. Rev. B*, **85**(24):241308, June 2012.

[Qi11] Xiao-Liang Qi. "Generic Wave-Function Description of Fractional Quantum Anomalous Hall States and Fractional Topological Insulators." *Physical Review Letters*, **107**(12):126803, September 2011.

[QZ11] Xiao-Liang Qi and Shou-Cheng Zhang. "Topological insulators and superconductors." *Reviews of Modern Physics*, **83**(4):1057–1110, October 2011.

[RBB09] Andreas Roth, Christoph Brüne, Hartmut Buhmann, Laurens W. Molenkamp, Joseph Maciejko, Xiao-Liang Qi, and Shou-Cheng Zhang. "Nonlocal transport in the quantum spin Hall state." *Science (New York, N.Y.)*, **325**(5938):294–297, July 2009.

[RH17] Rahul Roy and Fenner Harper. "Periodic table for Floquet topological insulators." *Physical Review B*, **96**(15):155118, October 2017.

[RH19] R. Roy and F. Harper. "private communications.", 2019.

[Roy09] Rahul Roy. "${Z}_{2}$ classification of quantum spin Hall systems: An approach using time-reversal invariance." *Physical Review B*, **79**(19):195321, May 2009.

[Roy10] Rahul Roy. "Characterization of three-dimensional topological insulators by two-dimensional invariants." *New Journal of Physics*, **12**(6):065009, June 2010.

[Roy14] Rahul Roy. "Band geometry of fractional topological insulators." *Phys. Rev. B*, **90**(16):1–7, October 2014.

[SCN04] Jairo Sinova, Dimitrie Culcer, Q. Niu, N. A. Sinitsyn, T. Jungwirth, and A. H. MacDonald. "Universal Intrinsic Spin Hall Effect." *Physical Review Letters*, **92**(12):126603, March 2004.

[Sem84] Gordon W. Semenoff. "Condensed-Matter Simulation of a Three-Dimensional Anomaly." *Physical Review Letters*, **53**(26):2449–2452, December 1984.

[Sim83] Barry Simon. "Holonomy, the Quantum Adiabatic Theorem, and Berry's Phase." *Physical Review Letters*, **51**(24):2167–2170, December 1983.

[SSH79] W. P. Su, J. R. Schrieffer, and A. J. Heeger. "Solitons in Polyacetylene." *Physical Review Letters*, **42**(25):1698–1701, June 1979.

[STG99] Horst L. Stormer, Daniel C. Tsui, and Arthur C. Gossard. "The fractional quantum Hall effect." *Reviews of Modern Physics*, **71**(2):S298–S305, March 1999.

[Str82] P. Streda. "Quantised Hall effect in a two-dimensional periodic potential." *Journal of Physics C: Solid State Physics*, **15**(36):L1299, December 1982.

[Tho70] D. J. Thouless. "Anderson's theory of localized states." *Journal of Physics C: Solid State Physics*, **3**(7):1559–1566, July 1970.

[Tho81] D. J. Thouless. "Localisation and the two-dimensional Hall effect." *Journal of Physics C: Solid State Physics*, **14**(23):3475–3480, August 1981.

[Tho84] D J Thouless. "Wannier functions for magnetic sub-bands." *Journal of Physics C: Solid State Physics*, **17**(12):L325–L327, April 1984.

[TKN82] D. J. Thouless, M. Kohmoto, M. P. Nightingale, and M. den Nijs. "Quantized Hall Conductance in a Two-Dimensional Periodic Potential." *Physical Review Letters*, **49**(6):405–408, August 1982.

[TSG82] D. C. Tsui, H. L. Stormer, and A. C. Gossard. "Two-Dimensional Magnetotransport in the Extreme Quantum Limit." *Physical Review Letters*, **48**(22):1559–1562, May 1982.

[Wan37] Gregory H. Wannier. "The Structure of Electronic Excitation Levels in Insulating Crystals." *Physical Review*, **52**(3):191–197, August 1937.

[WK78] Jun-ichi Wakabayashi and Shinji Kawaji. "Hall Effect in Silicon MOS Inversion Layers under Strong Magnetic Fields | Journal of the Physical Society of Japan." *Journal of the Physical Society of Japan*, **44**:1839–1849, June 1978.

[YKE08] Yue Yin, D. E. Katsanos, and S. N. Evangelou. "Quantum walks on a random environment." *Physical Review A*, **77**(2):022302, February 2008.